



Implantation of engineered adipocytes suppresses tumor progression in cancer models

Received: 19 November 2024

Accepted: 19 December 2024

Published online: 04 February 2025

Check for updates

Hai P. Nguyen^{1,2,3,14}, Kelly An^{1,2}, Yusuke Ito^{1,2}, Bhushan N. Kharbikar¹,
Rory Sheng^{1,2}, Breanna Paredes^{1,2}, Elizabeth Murray^{1,2}, Kimberly Pham^{1,2},
Michael Bruck^{1,2}, Xujia Zhou^{1,2}, Cassandra Biellak^{1,2}, Aki Ushiki^{1,2},
Mai Nobuhara^{1,2}, Sarah L. Fong^{1,2}, Daniel A. Bernards¹, Filipa Lynce^{1,2,5,6},
Deborah A. Dillon⁷, Mark Jesus M. Magbanua^{1,8}, Laura A. Huppert⁴,
Heinz Hammerlindl⁹, Jace Anton Klein^{1,3}, Luis Valdiviez¹⁰, Oliver Fiehn^{1,10},
Laura Esserman^{1,11}, Tejal A. Desai^{1,12}, Sook Wah Yee^{1,2},
Jennifer M. Rosenbluth^{4,13} & Nadav Ahituv^{1,2,✉}

Tumors exhibit an increased ability to obtain and metabolize nutrients. Here, we implant engineered adipocytes that outcompete tumors for nutrients and show that they can substantially reduce cancer progression, a technology termed adipose manipulation transplantation (AMT). Adipocytes engineered to use increased amounts of glucose and fatty acids by upregulating *UCP1* were placed alongside cancer cells or xenografts, leading to significant cancer suppression. Transplanting modulated adipose organoids in pancreatic or breast cancer genetic mouse models suppressed their growth and decreased angiogenesis and hypoxia. Co-culturing patient-derived engineered adipocytes with tumor organoids from dissected human breast cancers significantly suppressed cancer progression and proliferation. In addition, cancer growth was impaired by inducing engineered adipose organoids to outcompete tumors using tetracycline or placing them in an integrated cell-scaffold delivery platform and implanting them next to the tumor. Finally, we show that upregulating *UPP1* in adipose organoids can outcompete a uridine-dependent pancreatic ductal adenocarcinoma for uridine and suppress its growth, demonstrating the potential customization of AMT.

Tumors are complex tissues composed of cancerous and non-cancerous cells in a hypoxic and nutrient-deprived microenvironment. The tumor microenvironment contains heterogeneous cell populations, including immune cells, mesenchymal support cells and matrix components that contribute to tumor growth and progression¹. To survive this environment, tumors are capable of reprogramming metabolic pathways to better use available substrates in the surrounding tumor microenvironment, ultimately becoming dependent on these pathways for continued

growth and survival². In contrast to normal cells, the main pathway of glucose metabolism in cancer cells is aerobic glycolysis, termed the Warburg effect³. Glucose uptake and lactate production are increased in these cells, even in the presence of oxygen and functional mitochondria³. The increase in glycolytic flux allows glycolytic intermediates to supply subsidiary pathways to fulfil the metabolic demands of proliferating cells. During hypoxia, cancer cells also undergo metabolic reprogramming to increase lipid use, as fatty acids produce twice the energy of glucose^{4,5}.

A full list of affiliations appears at the end of the paper. ✉ e-mail: nadav.ahituv@ucsf.edu

There have been many efforts to target cancer glucose and fatty acid metabolism for therapeutic purposes. For glycolysis, these include drugs that target hexokinase 2 (HK2), which is involved in the initial steps in glycolysis, using ATP from the mitochondria to phosphorylate glucose, or drugs that target glucose transporters (GLUT1 and GLUT4)^{2,6–8}. Several drugs are also used to target lipid metabolism in cancer^{9–12}. These include drugs that target lipid uptake (targeting proteins such as LXR, CD36 and FABP4/5), lipogenic enzymes (such as ACC, ACLY, FASN and SCD1) and proteins involved in intracellular lipid homeostasis (such as CPT1A, PPARC and others)^{13,14}. In addition, recent work has shown that cold activation of brown adipose tissue (BAT), which dissipates energy by non-shivering thermogenesis, increases adipocyte glucose uptake and lipid metabolism and significantly inhibits tumor growth¹⁵. However, situating cancer patients in cold conditions for extended periods is challenging.

Here, we set out to develop a therapeutic approach, termed adipose manipulation transplantation (AMT), that uses two unique abilities of white adipose tissue (WAT). First, it can be readily extracted in the clinic by liposuction and implanted through reconstructive surgery; second, it can change into a BAT-like tissue, called browning or beiging^{16,17}, by upregulating essential transcriptional regulators or enzymes, such as the uncoupling protein 1 (*UCP1*), PPAR coactivator 1 alpha (*PPARGC1A*) or PR/SET domain 16 (*PRDM16*) genes^{18–33}. Similar to BAT, beige adipocytes have the capacity to convert energy to heat and contribute to whole-body energy expenditure³⁴. We show that CRISPR activation (CRISPRa) of either *UCP1*, *PRDM16* or *PPARGC1A* induces browning, subsequently increasing glucose and fat metabolism in human white adipocytes and adipose organoids. Co-culturing of these CRISPRa-modulated adipocytes with various cancer cell lines (breast, colon, pancreatic or prostate cancer) significantly suppresses cancer cell proliferation as well as decreases glucose uptake, glycolysis and fatty acid oxidation (FAO) capacity in the cancer cells. Subcutaneously co-transplanting CRISPRa-modulated human adipose organoids and cancer cell xenografts (two different breast cancer lines, pancreatic or prostate) into immune-compromised mice leads to significantly reduced tumor size with decreased hypoxia and angiogenesis. Implantation of engineered adipose organoids into pancreatic or breast cancer genetic mouse models significantly suppresses cancer progression. Furthermore, in the breast cancer model, we show that their implantation both near and distal to the tumor leads to similar results. To further demonstrate the therapeutic potential of this approach, we show that adipocytes isolated from resected human breast tissues can be similarly manipulated with CRISPRa and can inhibit the growth of patient-derived breast cancer organoids as well as the proliferation of high-risk non-cancerous breast tissues such as those from patients with *BRCA1/2* mutations. In addition, we also show how induction of CRISPRa using tetracycline or the implantation of modulated adipose organoids in an integrated cell-scaffold delivery platform can control this therapeutic approach in a reversible manner. Finally, to show that this approach can be customizable for other tumor-associated metabolic programs, we show how CRISPRa upregulation of uridine phosphorylase 1 (*UPP1*) in adipose organoids can suppress xenograft growth of a uridine-dependent pancreatic ductal adenocarcinoma (PDA)³⁵. Combined, our results introduce a cancer therapeutic approach that has the potential to treat numerous cancer types.

Results

CRISPRa browning of human white adipocytes

To induce browning in human adipocytes, we used CRISPRa to upregulate *UCP1*, *PPARGC1A* or *PRDM16*, all known genes involved in BAT development and function. Using CRISPR³⁶, we designed five guide RNAs (gRNAs) targeting each gene's promoter and cloned them into an adeno-associated virus (AAV)-based expression vector. Differentiated adipocytes derived from human white preadipocytes were co-transfected with the gRNAs along with a *Staphylococcus aureus*

endonuclease-deficient Cas9 (dCas9) fused to the VP64 transcriptional activator. We used an *S. aureus* dCas9 due to its smaller size and the VP64 transcriptional activator (which carries four copies of VP16, a herpes simplex virus type 1 transcriptional activator³⁷) because it provides moderate gene upregulation and is small enough to fit into AAV, which has a 4.7 kb optimal packaging capacity³⁸. To generate mature human adipocytes, preadipocytes were subjected to adipocyte differentiation using a cocktail of 3-isobutyl-1-methylxanthine (IBMX), dexamethasone and insulin before being subjected to CRISPRa. After 4 days, we measured gene expression by quantitative PCR with reverse transcription (RT-qPCR), finding several gRNAs to significantly increase the expression levels of *UCP1*, *PPARGC1A* and *PRDM16* in the transfected cells compared to the control cells (treated with dCas9–VP64 only) (Extended Data Fig. 1a). We selected the top two gRNAs for each gene for AAV serotype 9 (AAV9) packaging. We used AAV9 because it was shown to effectively infect various adipose depots³⁹. We infected human differentiated adipocytes with these viruses along with AAV9 dCas9–VP64, finding for each gene at least one gRNA that significantly increased expression levels compared to the dCas9–VP64-only control (Extended Data Fig. 1b). We used the top-activating gRNA AAV for all subsequent experiments.

We next examined whether our CRISPRa treatment increases browning in these human white adipocytes. Human adipocytes transduced with the top gRNA for *UCP1*, *PRDM16* or *PPARGC1A* showed significantly increased expression of their target genes compared to dCas9–VP64-only infected cells (Extended Data Fig. 1c). In addition, we also observed increased mRNA levels for brown fat marker genes, including *TFAM*, *DIO2*, *CPT1b* and *NRF1* upon upregulation of either of the three genes (Extended Data Fig. 1d); *PRDM16* CRISPRa did not show upregulation of *CPT1b* and *NRF1*. We next examined the oxygen consumption rate (OCR) in these cells using Seahorse (Methods), by initially blocking oxygen consumption and then adding 1 μM oligomycin, followed by the introduction of 1 μM carbonyl cyanide-p-trifluoromethoxy-phenylhydrazone (FCCP) to measure the maximal respiratory capacity. We found that CRISPRa-AAV treatment targeting all these genes increased overall OCR levels in human white adipocytes, with *UCP1*-gRNA-AAV-treated cells having the largest increase (Extended Data Fig. 1e). In addition, these cells showed increased uncoupled respiration (under oligomycin, an ATP synthase inhibitor), indicating a brown fat-like phenotype (Extended Data Fig. 1e). CRISPRa-treated cells also had elevated maximal respiration following FCCP treatment (Extended Data Fig. 1e). Furthermore, these CRISPRa-AAV-engineering adipocytes showed increased glucose uptake in both basal and insulin-stimulated conditions (Extended Data Fig. 1f). We also tested the FAO capacity of these cells by performing a similar Seahorse OCR assay. In both BSA and BSA-conjugated-palmitate (saturated fatty acid complex) media, we found that our CRISPRa-treated adipocytes had an overall OCR increase in BSA-conjugated-palmitate (Extended Data Fig. 1g). Under FCCP treatment, in which the increase of OCR in palmitate-containing media compared to BSA-containing media is thought to be caused by exogenous FAO, we found that upregulation of either gene increased exogenous FAO capacity in human adipocytes (Extended Data Fig. 1h). Similarly, *UCP1*-upregulated human adipocytes had the largest increase in FAO. We also found that *UCP1*-upregulated human adipocytes had higher fatty acid uptake than the dCas9–VP64 control cells (Extended Data Fig. 1i). Taken together, we show that AAV-based CRISPRa upregulation of *UCP1*, *PPARGC1A* or *PRDM16* induces browning in human adipocytes, leading them to have increased glucose uptake and FAO.

CRISPRa-modulated adipocytes suppress tumor growth in vitro

We next evaluated whether our CRISPRa ‘browned’ adipocytes could inhibit cancer growth in vitro using a co-culturing system (Fig. 1a). We initially treated differentiated adipocytes with CRISPRa-AAV for either

of the three genes (*UCP1*, *PPARGC1A* or *PRDM16*) and replated these adipocytes on the top chamber of a 12-well or 24-well Transwell plate, which has inserts of 0.4 µm membranes, so that the adipocytes did not contact the cells on the lower chamber (Fig. 1a). In the lower chamber, we grew five different cancer cell lines: breast cancer cells MCF-7 (estrogen receptor-positive (ER⁺), progesterone receptor-positive (PR⁺), glucocorticoid receptor-positive (GR⁺)) and MDA-MB-436 (triple negative), colon cancer (SW-1417), pancreatic cancer (Panc 10.05) and prostate cancer (DU-145). As a negative control, we used adipocytes infected with dCas9-VP64 only. After 3 days, we observed that all five cancer cell lines that were co-cultured with *UCP1*, *PPARGC1A* or *PRDM16* CRISPRa-treated human adipocytes showed significantly lower cell numbers than cancer cells co-cultured with dCas9-VP64-treated adipocytes (Fig. 1b). We also found that the number of cancer cells co-cultured with CRISPRa-treated adipocytes was threefold to five-fold lower than cancer cells co-cultured with the control adipocytes (Fig. 1c). By RT-qPCR, we observed that all cancer cells co-cultured with CRISPRa-treated adipocytes had significantly reduced levels of the proliferation marker *MKI67* (other than Panc 10.05 and DU-145 treated with *PRDM16* CRISPRa) compared to control cells, with *UCP1*-CRISPRa having the greatest effect (Fig. 1d). We also performed a BrdU incorporation assay, finding that after 24 h, CRISPRa co-cultured cancer cells showed significantly reduced proliferation compared to cells co-cultured with control adipocytes (Extended Data Fig. 1j).

We next analyzed the glucose and fatty acid metabolism of the co-cultured cancer cells. To measure glycolysis, we used the extracellular acidification rate (ECAR) assay in which the basal glycolytic rate is measured by adding glucose and the maximal glycolytic rate is measured by oligomycin A addition. We found that most cancer cell lines co-cultured with CRISPRa-AAV-treated adipocytes showed a significant reduction in both basal and maximal glycolytic rate (Fig. 1e,f) and lower glucose uptake in both basal and insulin conditions (Fig. 1g,h). Using RT-qPCR, we also found that the expression of key glycolysis genes, such as *GCK* and *GLUT4*, a major glucose transporter, was significantly lower in most cancer cells co-cultured with CRISPRa-AAV adipocytes than in the negative control (Fig. 1i). We also examined FAO using Seahorse. In BSA-only media, we found that all cancer cell lines that were co-cultured with *UCP1*-CRISPRa-modulated adipocytes had lower OCR. For *PPARGC1A* and *PRDM16* CRISPRa-modulated adipocytes, this was only observed in MDA-MB-436 and Panc 10.05 cells (Extended Data Fig. 1k). In palmitate-containing media, we found that all five cancer cell lines that were co-cultured with CRISPRa-AAV adipocytes had reduced FAO compared to the negative control (Fig. 1l). Moreover, using RT-qPCR, we found in several CRISPRa conditions that the cancer cells had lower expression of both *CD36*, a fatty acid transporter on the cell membrane, and *CPT1b*, a key regulator of FAO in the mitochondria, further confirming decreased FAO (Fig. 1m). To show that this approach works with other adipocyte lines, we also upregulated *UCP1* in human adipocytes differentiated from primary preadipocytes (Extended Data Fig. 1l) and found that they inhibit tumor growth of all five cancer cells (Extended Data Fig. 1m). Combined, our data shows that our CRISPRa-modulated adipocytes reduce

glycolysis and FAO in five different cancer cell lines and can significantly suppress cancer growth.

We next compared the tumor suppression capability of CRISPRa-AAV-modulated adipocytes to known metabolic cancer drugs. We grew MCF-7 cells and treated them with the following: (1) CRISPRa-*UCP1*-AAV adipocytes at the top layer of a Transwell model; (2) 6-aminonicotinamide, which is known to target glycolysis and reduce cell growth in a variety of tumors^{40–42}, including MCF-7 breast cancer cells⁴¹, using similar or higher drug concentrations (50 µM, 100 µM and dimethylsulfoxide (DMSO) as a control)⁴¹; and (3) etomoxir, an inhibitor of FAO⁴³ that suppresses tumor cell growth^{44,45}, including breast cancer^{46,47}, using concentrations previously used for MCF-7 cells (100 µM, 200 µM and DMSO as a control)⁴⁷. Using a luminescent cell viability assay (Methods), we observed an increased reduction in the number of cancer cells cultured with CRISPRa-*UCP1*-AAV adipocytes compared to 6-aminonicotinamide and a slightly increased reduction compared to etomoxir (two-tailed *t*-test *P* = 0.0163 versus *P* = 0.0319 for CRISPRa-*UCP1*-AAV or etomoxir, respectively; Extended Data Fig. 1n).

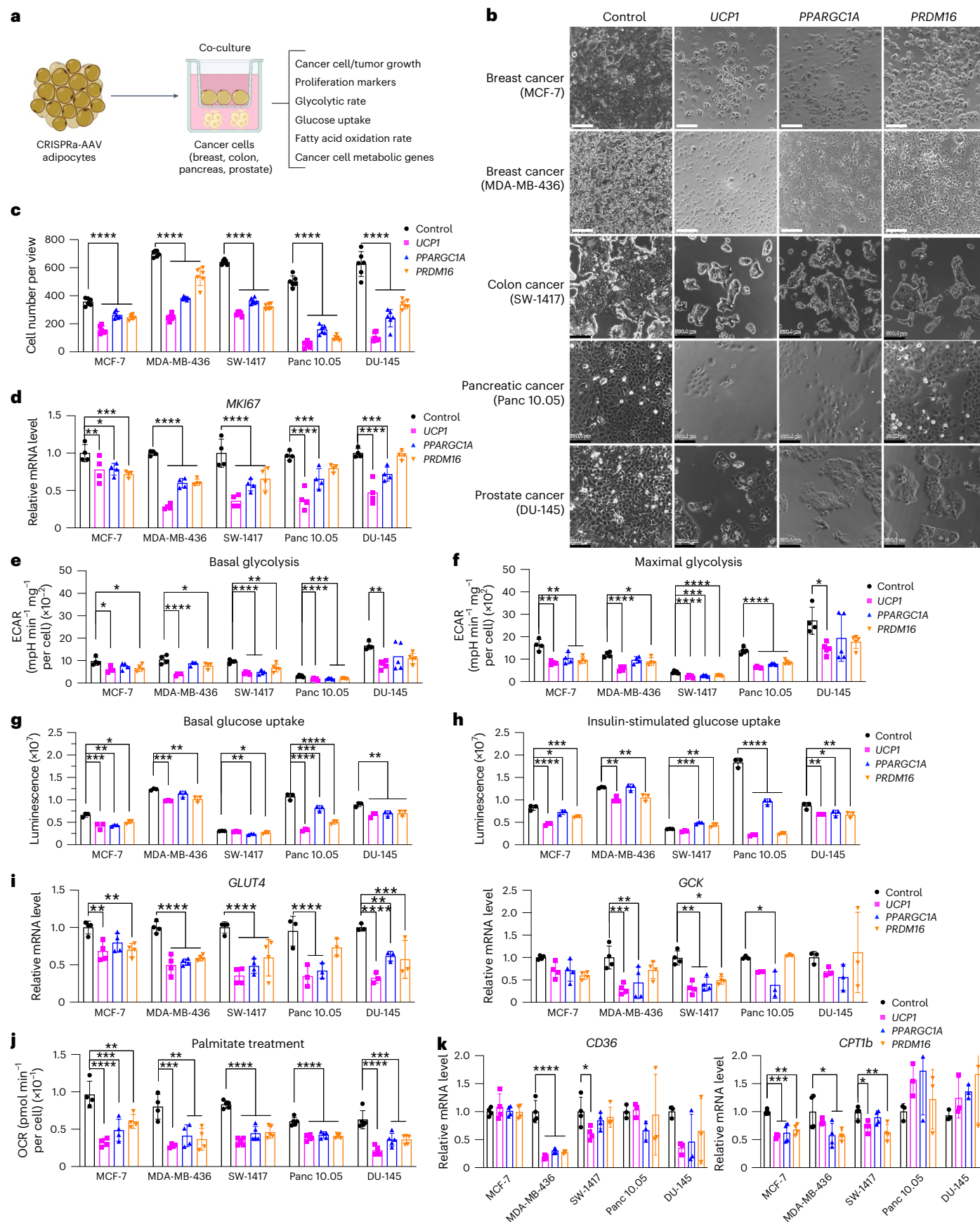
Modulated human adipose organoids suppress xenograft growth

To examine whether CRISPRa-modulated adipocytes could inhibit cancer growth in tumor xenograft models, we co-transplanted four cancer cell lines (MCF-7 and MDA-MB-436 (breast), Panc 10.05 (pancreas) and DU-145 (prostate)) with CRISPRa-modulated human adipose organoids. Although adipocytes could be used for co-transplantation, adipose organoids offer added advantages, such as providing a three-dimensional (3D) culture that can better recapitulate the heterogeneity of adipose tissue, enhanced response to endogenous stimuli and the ability to form tissue microenvironments that could better integrate with cancer cells following transplantation. We initially established culturing conditions for human adipose organoids. We used immortalized human preadipocytes grown using methods that combine features from three different 3D culturing protocols^{48,49}. In brief, we cultured human preadipocytes in basal DMEM media supplemented with 10% FBS in Nunc 96-well plates treated with Nunclon Delta. Organoids formed after 48 h and were then differentiated into adipose organoids using a differentiation cocktail containing IBMX, dexamethasone, insulin, T3 and rosiglitazone. Adipocytes formed 21 days post differentiation (Extended Data Fig. 2a). Using RT-qPCR, we analyzed these organoids for various adipogenic markers, including *FABP4*, *PLIN1* and *ADIPOQ*, finding all to be expressed (Extended Data Fig. 2b). We further tested our ability to upregulate *UCP1*, *PPARGC1A* and *PRDM16* in these organoids using similar methods and AAV gRNAs as in the adipocytes, finding all three genes to show significant upregulation of the target genes (Extended Data Fig. 2c). With the establishment of these adipose organoid-culturing and CRISPRa conditions, we next set out to test whether they can suppress xenograft cancer growth.

To generate xenografts, cancer cells were subcutaneously implanted into immuno-compromised SCID mice. After 6–8 weeks, *UCP1*-CRISPRa-treated human adipose organoids were mixed with Matrigel and co-transplanted adjacent to palpable tumors. For all subsequent

Fig. 1 | CRISPRa-modulated adipocytes inhibit cancer cell growth in vitro. **a**, Schematic of the co-culturing model of cancer cells and CRISPRa-treated adipocytes using Transwell plates and their subsequent phenotyping (created with BioRender.com). **b**, Representative images of cancer cells, including breast (MCF-7, MDA-MB-436), colon (SW-1417), pancreatic (Panc 10.05) and prostate cancer (DU-145), that were co-cultured with CRISPRa-upregulating *UCP1*, *PPARGC1A* and *PRDM16* or control (dCas9-VP64 only) adipocytes. Scale bars, 530.4 µm. **c**, Cancer cell number per view of image (four images or replicates per condition). **d**, RT-qPCR of the proliferation marker gene *MKI67* for cancer cells co-cultured with CRISPRa-modulated adipocytes (*n* = 4 biological replicates). **e**, Basal glycolysis measured by calculating the area under the curve of ECAR upon glucose treatment (*n* = 4–5 biological replicates). **f**, Maximal glycolysis

measured by calculating the area under the curve of ECAR upon oligomycin treatment (*n* = 4–5 biological replicates). **g, h**, Glucose uptake of cancer cells co-cultured with CRISPRa-modulated adipocytes without (g) or with (h) insulin (*n* = 3 biological replicates). **i**, RT-qPCR of glucose transporter *GLUT4* and glycolytic enzyme *GCK* in cancer cells (*n* = 3–4 biological replicates). **j**, Exogenous FAO of cancer cells calculated by the difference of area under the curve of OCR of BSA-palmitate media upon FCCP treatment (*n* = 4 biological replicates). **k**, RT-qPCR of fatty acid transporter *CD36* and fatty acid regulatory transporter *CPT1b* in cancer cells that were co-cultured with CRISPRa-treated adipocytes (*n* = 3–4 biological replicates). All statistical tests were carried out using a one-way ANOVA and data are represented as mean ± s.d. **P* ≤ 0.05; ***P* ≤ 0.01; ****P* ≤ 0.001; *****P* ≤ 0.0001.



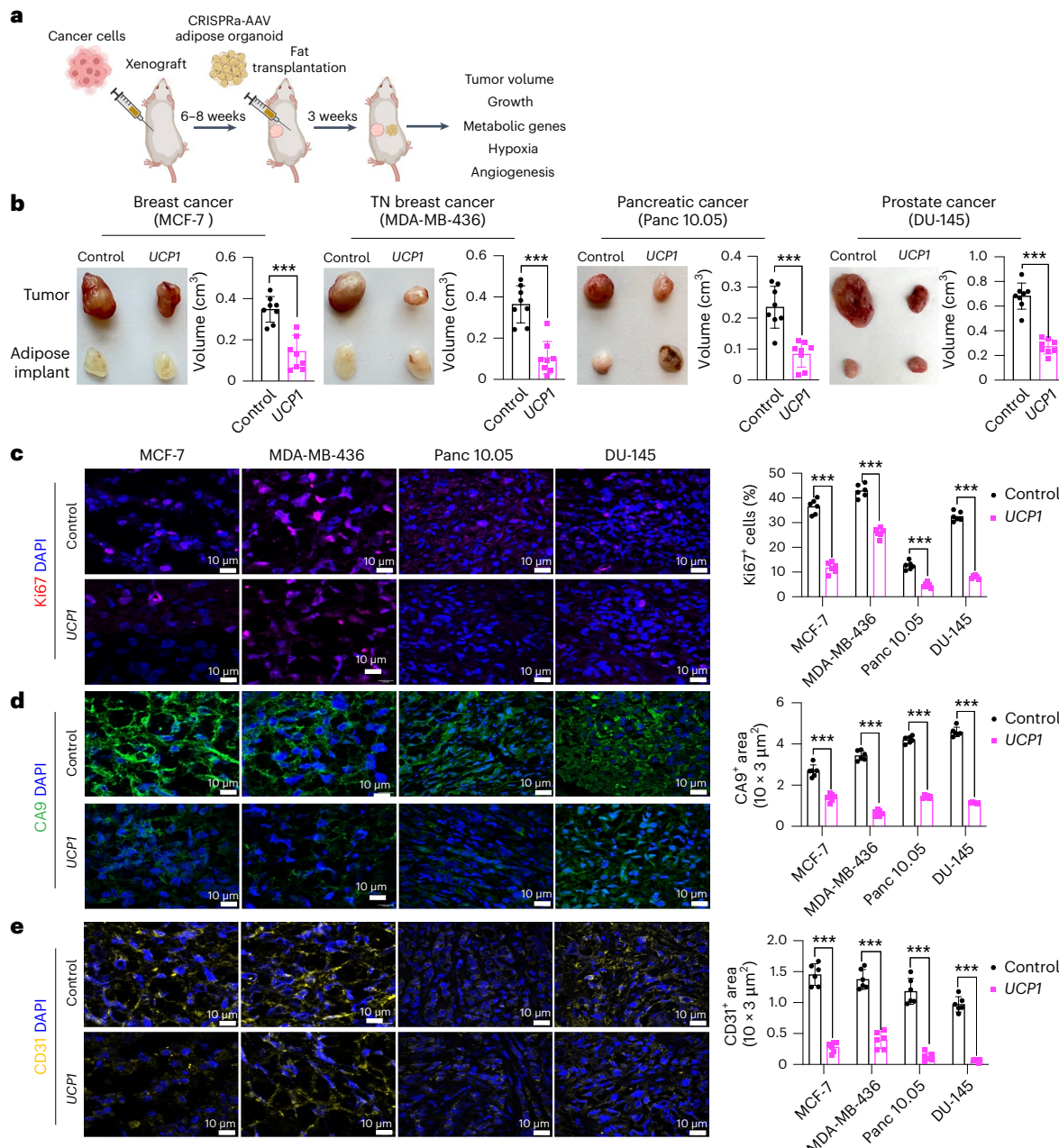


Fig. 2 | Co-transplantation of xenografts with *UCP1*-CRISPRa-modulated human adipose organoids suppresses tumor growth. **a**, Schematic of the co-transplantation model for xenografts and *UCP1*-CRISPRa-treated human adipose organoids in immune-deficient SCID mice and their subsequent phenotyping (created with BioRender.com). **b**, Representative images of xenograft tumors from various cancer cell lines, including breast (MCF-7 and MDA-MB-436), pancreatic (Panc 10.05) and prostate cancer (DU-145), that were co-transplanted with *UCP1*-CRISPRa human adipose organoids or control (dCas9-VP64 only).

adipose organoids ($n = 8$ mice per treatment). TN, triple negative. The bar chart to the right of the images shows the volume of xenograft tumors that were co-transplanted with *UCP1*-CRISPRa human adipose organoids compared to control (dCas9-VP64 only) ($n = 6–8$ mice). **c–e**, Immunofluorescence staining and quantification of Ki67 (**c**), CA9 (**d**) and CD31 (**e**) in cryosections of xenograft tumors ($n = 4–5$ sections per treatment). Scale bars, 10 μm. All statistical tests were carried out using a two-tailed *t*-test and data are represented as mean ± s.d. *** $P \leq 0.001$.

assays, we only used *UCP1*-CRISPRa, as it showed the most optimal results in our cell culture experiments. Some reports have suggested that brown fat could be linked to cancer-associated cachexia (loss of skeletal muscle and fat)⁵⁰; therefore, each week we measured the body weight of mice co-transplanted with cancer cells and *UCP1*-modulated adipose organoids. We found no significant differences in body weight between CRISPRa-treated and control mice (Extended Data Fig. 2d). Tumors and human adipose organoids were collected after 3 weeks (Fig. 2a). Adipose organoids were stained with Lipid-Tox, showing adipocytes were still present in them 3 weeks after

implantation (Extended Data Fig. 2e). These organoids also had increased gene expression levels of *UCP1*, some brown fat genes including *PPARGC1A* and *CPT1b* and the *GLUT4* glucose transporter compared to control adipose organoids (Extended Data Fig. 2f). All tumor types co-transplanted with CRISPRa-modulated human adipose organoids were significantly smaller than dCas9-VP64-only transplanted human adipose organoids, having over 50% reduction in volume (Fig. 2b). Gene analysis showed that tumors co-transplanted with CRISPRa-treated adipose organoids had decreased expression of the proliferation marker gene *MKI67* (Extended Data Fig. 2g) as well as

reduced marker gene expression for glycolysis (*GLUT4* (except for DU-145), *GCK*) and FAO (*CD36* (except for DU-145), *CPT1B*) (Extended Data Fig. 2h). Using immunofluorescence, we examined additional tumor marker genes and found that all tumors co-transplanted with *UCP1*-CRISPRa-modulated human adipose organoids had markedly reduced Ki67⁺ cells (Fig. 2c). In addition, cancer cells showed decreased levels of hypoxia, identified by having a lower carbonic anhydrase (CA9⁺) area per image view (Fig. 2d). Furthermore, these tumors exhibited decreased levels of CD31⁺ area per image view, indicating reduced microvessel density and suggesting a corresponding lower metastatic potential (Fig. 2e). We also found higher levels of caspase-3⁺ in both MCF-7 and MDA-MB-436 xenografts co-implanted with *UCP1*-CRISPRa adipose organoids compared to controls, indicating higher apoptotic rates (Extended Data Fig. 2i). To show that this approach can work with another adipocyte cell line, we repeated these experiments for MCF-7 xenografts with *UCP1*-CRISPRa primary adipocytes and found that they also significantly suppressed tumor growth (Extended Data Fig. 2j). Taken together, these results show that *UCP1*-CRISPRa-modulated human adipose organoids significantly reduce glycolysis and FAO, reduce hypoxia and inhibit tumor growth for four different cancer types *in vivo*.

Modulated adipose organoids outcompete tumors for nutrients

We next set out to characterize the effect of *UCP1*-CRISPRa adipose organoids on various metabolic parameters and test whether resource competition is involved in the observed cancer suppression. We implanted *UCP1*-CRISPRa or dCas9–VP64 only (negative control) adipose organoids in SCID mice and, after 6 weeks, used the comprehensive lab animal monitoring system (CLAMS) to measure their whole-body oxygen consumption. Mice implanted with *UCP1*-CRISPRa adipose organoids exhibited increased whole-body oxygen consumption at all temperatures (Extended Data Fig. 3a). We also carried out both a glucose and insulin tolerance test on these mice, which revealed that all *UCP1*-CRISPRa-treated mice had increased glucose tolerance and insulin sensitivity (Extended Data Fig. 3b). Following up on these results, we next examined the insulin plasma levels in all four of our xenograft lines, which showed that mice co-transplanted with *UCP1*-CRISPRa adipose organoids had significantly lower insulin levels than those co-transplanted with dCas9–VP64 control adipose organoids and were comparable to levels of wild-type SCID mice (Extended Data Fig. 3c). Combined, these data suggest that *UCP1*-CRISPRa-modulated adipose organoids lead to robust energy consumption, enhanced glucose tolerance and insulin sensitivity and reduced insulin levels.

To examine whether *UCP1*-modulated adipose organoids can prevent glucose uptake in the co-transplanted xenograft tumor, we measure glucose levels in both the adipose organoids and co-implanted MCF-7 tumor. We found that *UCP1*-modulated adipose organoids had higher

glucose levels than controls and that xenograft tumors co-implanted with *UCP1*-modulated adipose organoids had lower levels of glucose than control tumors (Fig. 3a and Supplementary Table 1). Metabolomics analysis of these tumors found that glucose levels and glycolytic intermediates, including glucose-6-phosphate, fructose-6-phosphate, 3-phosphoglycerate and phosphoenolpyruvate, were lower in the tumors co-implanted with *UCP1*-modulated adipose organoids than in the control tumors (Fig. 3b and Supplementary Table 1). In addition, the tumors co-implanted with *UCP1*-modulated adipose organoids had lower fatty acid levels, including oleic acid and palmitoleic acid, than the control tumors (Fig. 3c and Supplementary Table 1).

To further test whether nutrient competition is contributory to the ability of *UCP1*-CRISPRa-treated adipose organoids to suppress tumor growth, we performed similar MCF-7 xenograft experiments with mice fed with either standard chow, a high-fat diet (HFD) or 15% glucose containing water (Fig. 3d). We found that tumors co-implanted with *UCP1*-CRISPRa adipose organoids from mice fed with standard chow had significantly lower volume than mice co-implanted with control (dCas9–VP64 only) (Fig. 3e and Extended Data Fig. 3c), which showed significant reduction in volume starting 2 weeks post implantation (Extended Data Fig. 3d). By contrast, HFD-treated or 15% glucose-treated mice showed no apparent difference in tumor growth compared to the negative control (Fig. 3e). Analysis of tumors from mice on a HFD or 15% glucose found that they had expression patterns of the *MKI67* proliferation marker, glycolysis (*GLUT4*, *GCK*) and FAO (*CD36*, *CPT1B*) that are similar to the negative control, whereas mice on a regular chow diet had significantly lower expression for all these markers (Fig. 3f). Similarly, tumors from mice fed with standard chow displayed reduced levels of Ki67⁺ cells, CA9⁺ area, and CD31⁺ area compared to controls, whereas there was no apparent difference in tumors from HFD-treated or 15% glucose-treated mice (Fig. 3g-i and Extended Data Fig. 3e).

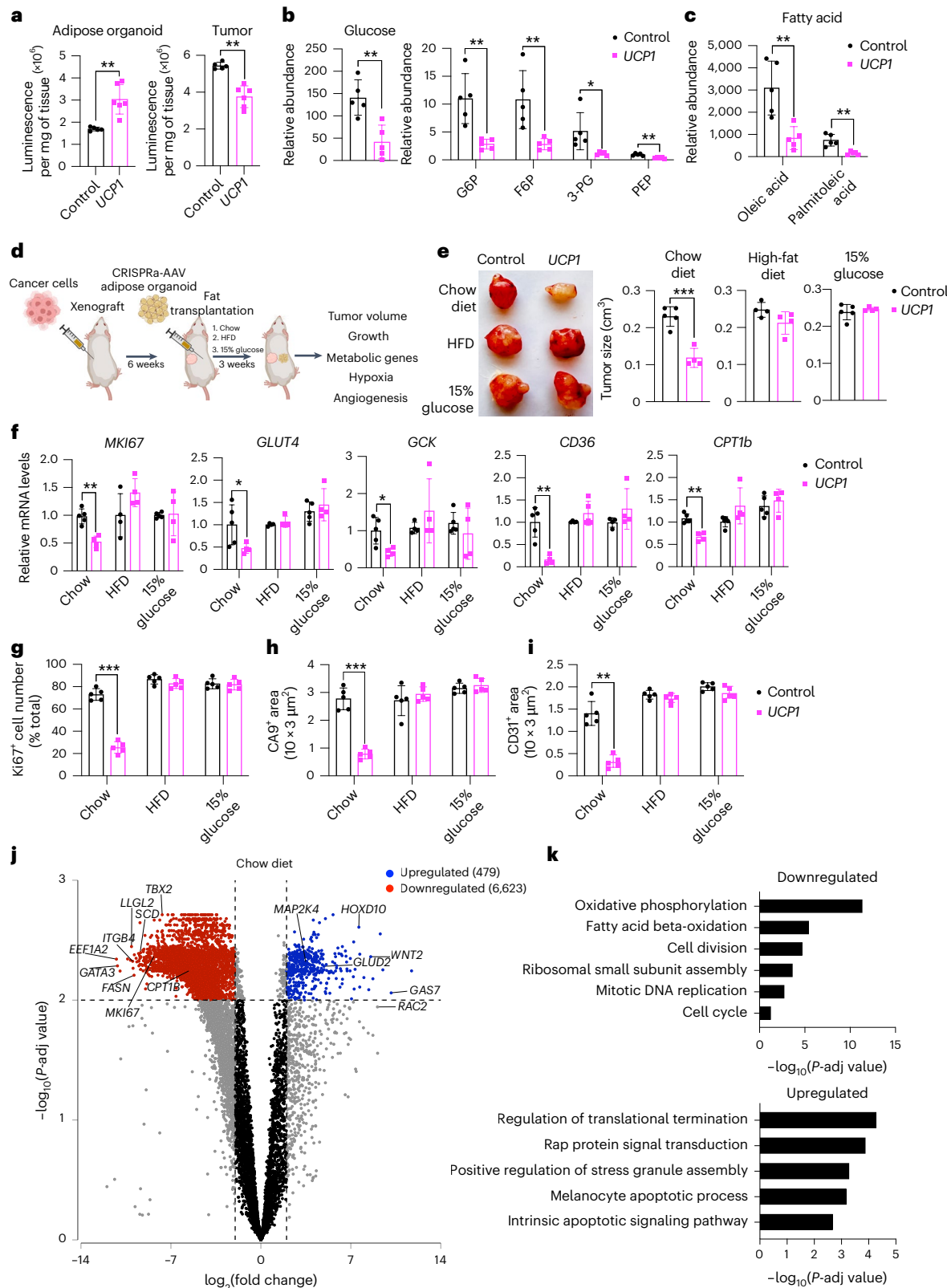
We next performed RNA-seq on tumors from all conditions (standard chow, HFD, 15% glucose and negative controls). Principal component analysis revealed that tumors co-implanted with *UCP1*-CRISPRa-modulated adipose organoids in mice fed with a standard chow diet were significantly different than controls, whereas there was no consistent difference in tumors co-implanted with *UCP1*-CRISPRa-modulated adipose organoids and control tumors in mice fed with HFD or 15% glucose water (Extended Data Fig. 3f). Tumors co-implanted with *UCP1*-CRISPRa-modulated adipose organoids in mice fed with a standard chow diet had significantly more global gene expression changes (7,102 differentially expressed genes with 6,623 downregulated and 479 upregulated genes) (Fig. 3j) compared to zero genes for mice treated with a HFD or 15% glucose water (Extended Data Fig. 3g). Among the downregulated genes in the standard chow tumors co-implanted with *UCP1*-CRISPRa-modulated adipose organoids, we found many metabolic genes, including *CPT1b*, *SCD*

Fig. 3 | Increasing nutrients reduces *UCP1*-CRISPRa human adipose organoid cancer suppression. **a**, Glucose levels measured from adipose organoids co-transplanted with MCF-7 xenograft tumors using a glucose uptake assay ($n = 5\text{--}6$ biological replicates). **b,c**, Metabolomics analysis of glucose and glycolysis intermediates, including glucose-6-phosphate (G6P), fructose-6-phosphate (F6P), 3-phosphoglycerate (3-PG) and phosphoenolpyruvate (PEP) (**b**), and fatty acids, including oleic acid and palmitoleic acid ($n = 5$ biological replicates) (**c**). Data are represented as mean \pm s.d. **d**, Schematic of the co-transplantation model for MCF-7 tumor xenograft and *UCP1*-CRISPRa-treated human adipose organoids in immune-deficient SCID mice fed with standard chow, HFD or 15% glucose containing water and their subsequent phenotyping (created with BioRender.com). **e**, Representative images and tumor volume of MCF-7 xenografts that were co-transplanted with *UCP1*-CRISPRa human adipose organoids or control (dCas9–VP64 only) from mice on different diets ($n = 4\text{--}5$ mice per treatment). **f**, RT-qPCR of proliferation marker gene *MKI67* and metabolic genes (*GLUT4*, *GCK*, *CD36*, *CPT1b*) from MCF-7 xenograft tumors co-transplanted with

UCP1-CRISPRa or control (dCas9–VP64 only) human adipose organoids in mice fed with various diets ($n = 4\text{--}5$ biological replicates). **g-i**, Immunofluorescence quantification from cryosections of xenograft tumors ($n = 5$ sections per treatment) of Ki67 (**g**), CA9 (**h**) and CD31 (**i**). **j**, Volcano plot showing *P* value versus fold change of MCF-7 tumors co-implanted with *UCP1*-CRISPRa compared to negative-control-treated human adipose organoids in mice on standard chow diet. Differentially expressed genes are those exhibiting at least a \pm fourfold change, with their expression being significantly different from basal level (false discovery rate (FDR)-adjusted $P < 0.01$). **k**, Gene ontology enrichment of significantly downregulated and upregulated genes in MCF-7 tumors from mice on standard chow, using Geneontology.org (<https://geneontology.org>)^{62,63} with an FDR-adjusted Fisher's Exact test *P* value of <0.0001 . Cell cycle is represented by the term 'Cell cycle: positive regulation of G2/M transition of mitotic cell cycle', and cell division by the term 'Cell division: cytokinesis'. All statistical tests in **a-i** were carried out using a two-tailed *t*-test and data are represented as mean \pm s.d. * $P \leq 0.05$; ** $P \leq 0.01$; *** $P \leq 0.001$.

(stearoyl-CoA desaturase) and *FASN* (fatty acid synthase), and cancer growth and progression regulated genes, such as *MKI67*, *ITGB2* (ref. 51), *LLGL2* (ref. 52), *GATA3* (ref. 53), *EEF1A2* (refs. 54,55) and *TBX2* (ref. 56) (Fig. 3j). Upregulated genes included tumor suppressor genes, such as *HOXD10* (ref. 57), *GAS7* (ref. 58) and *MAP2K4* (ref. 59), and cancer progression genes, including *WNT2* (ref. 60) and *RAC2* (ref. 61) (Fig. 3j). We next performed gene ontology enrichment analysis

using Geneontology.org (<https://geneontology.org/>)^{62,63} on differentially expressed genes in tumors of mice fed with standard chow and found downregulated differentially expressed genes to be enriched in pathways involved in metabolic regulation, including FAO, oxidative phosphorylation, cell growth, DNA replication and cell division (Fig. 3k, top). Upregulated enriched pathways included those involved in cellular response to stress response and cell apoptosis (Fig. 3k, bottom).



We found no significant pathway changes in tumors in mice fed with HFD or 15% glucose water. In summary, these experiments suggest that *UCP1*-CRISPRa-modulated adipose organoids outcompete tumors for glucose and fatty acids, as increasing fatty acid or glucose levels abolished cancer suppression.

AMT suppresses cancer development in genetic mouse models

To examine whether our AMT approach can prevent cancer development, we used pancreatic and breast cancer genetic mouse models. For pancreatic cancer, we used the KPC mouse model that, upon tamoxifen treatment, develops PDA caused by conditional mutations in *Kras* and *Trp53* (ref. 64). For breast cancer, we used *MMTV-PyMT* mice on an FVB background, containing a mouse mammary tumor virus (*MMTV*) long terminal repeat upstream of the polyomavirus middle T antigen (*PyVmT*); these mice develop mammary tumors with a mean latency of 53 days⁶⁵. We first designed five gRNAs targeting the mouse *Ucp1* gene and transfected them into mouse 3T3-L1 adipocytes, finding all five to upregulate *Ucp1* (Extended Data Fig. 4a). We next selected two gRNA for AAV9 packaging and infected 3T3-L1 differentiated adipocytes with these viruses along with AAV9 dCas9–VP64, finding that all of them significantly increased *Ucp1* gene expression levels compared to dCas9–VP64-only control (Extended Data Fig. 4b). We used the top-activating gRNA AAV9 for all subsequent experiments. As organoids have several of the aforementioned advantages, we generated adipose organoids using mouse preadipocytes, using techniques similar to those described for human adipose organoids (Methods). We then infected them with AAV9 dCas9–VP64 and *Ucp1*-gRNA and observed both *mCherry* expression from our gRNA virus and significant *Ucp1* upregulation (Extended Data Fig. 4c).

We next set out to test whether we can suppress pancreatic cancer development using KPC mice. KPC mice were treated with tamoxifen on postnatal day 0–4. At 4 weeks of age, *Ucp1*-CRISPRa or dCas9–VP64-only (negative control) adipose organoids were orthotopically implanted next to the pancreas (Fig. 4a). After 6 weeks, the pancreases were removed and analyzed. Over those 6 weeks, we observed no significant difference in body weight between mice implanted with *Ucp1*-CRISPRa organoids or control organoids (dCas9–VP64 only) (Extended Data Fig. 4d). We found that KPC mice implanted with *Ucp1*-CRISPRa-upregulated adipose organoids had significantly smaller tumors than those in control dCas9–VP64-implanted mice (Fig. 4b), reduced pancreatic mass and *Ck19*⁺ staining (Fig. 4c and Extended Data Fig. 4e). They also showed reduced expression of the proliferation marker *Mki67* as well as genes involved in FAO (*Cd36*, *Cpt1b*) (Fig. 4d). In addition, we found *Ucp1*-CRISPRa mice to have lower expression levels of the pancreas' main glucose transporter, *Glut2*, but no significant change for the *Gck* glycolysis marker (Fig. 4d). *Ucp1*-CRISPRa mice also had a lower number of *Ki67*⁺ cells than control mice as determined by immunofluorescence (Fig. 4e and Extended Data Fig. 4e). In addition, we observed lower CA9⁺ and CD31⁺ area per image view in mouse tumors implanted with *Ucp1*-CRISPR adipose organoids, suggesting reduced hypoxia and angiogenesis (Fig. 4e and Extended Data Fig. 4e). These tumors also had slightly increased levels of caspase-3⁺ cells compared to controls (Extended Data Fig. 4f), suggesting increased apoptosis. Furthermore, we found *Ucp1*-CRISPRa adipose organoids of KPC mice to have significantly reduced insulin levels compared to control mice (Extended Data Fig. 4g).

To examine whether our treatment might provide systematic therapeutic effect in suppressing breast cancer growth, we next used *MMTV-PyMT* female mice, implanting *Ucp1*-CRISPRa or dCas9–VP64 adipose organoids near the third nipples of 4-week-old mice (Fig. 4f). Given that our experiments suggest a nutrient competition model and cold treatment was previously shown to cause widespread BAT activation and subsequent cancer suppression¹⁵, we also examined whether distal implantation of adipose organoids could suppress cancer development by implanting organoids in the back of 4-week-old

mice. At 6 weeks post implantation, tumors were dissected and analyzed. We found no difference in body weight of mice implanted with *Ucp1*-CRISPRa organoids compared to those implanted with control organoids (Extended Data Fig. 4h). Remarkably, we found that both strategies of organoid implantation resulted in significantly reduced tumor size (Fig. 4g) and volume (Fig. 4h) regardless of the site of implantation. Tumors also had decreased expression of the *Mki67* proliferation marker and metabolic genes *Glut4*, *Gck*, *Cd36* and *Cpt1b* (Fig. 4i). The tumors of mice implanted with *Ucp1*-CRISPRa adipose organoids had fewer *Ki67*⁺ cells than control mice (Fig. 4j). These tumors also had lower CA9⁺ and CD31⁺ area per image view and increased caspase-3⁺ (Fig. 4k–m), suggesting that they have reduced hypoxia and angiogenesis and increased apoptosis. Additionally, mice implanted with *Ucp1*-CRISPRa adipose organoids had significantly lower plasma insulin levels than control mice (Extended Data Fig. 4i). Taken together, our results indicate that our CRISPRa-modulated adipose organoids could have systematic therapeutic effects in suppressing cancer growth.

Breast dissected modulated adipocytes suppress tumor growth

To further demonstrate the therapeutic potential of AMT, we treated adipocytes obtained from dissected human breast tissues with *UCP1*-CRISPRa AAV9 and tested their ability to suppress tumor progression by co-culturing them with breast cancer organoids generated from dissected breast tumors or grown from metastatic pleural effusions (Fig. 5a). Samples were obtained from patients who underwent breast surgery or thoracentesis. For the co-culture experiments, we used five different breast cancer organoids generated from patients with early stage or metastatic triple-negative breast cancer (ER[−], PR[−] and human epidermal growth factor receptor 2-negative (HER2[−])) or hormone receptor-positive (ER⁺ and/or PR⁺), HER2[−] breast cancer (Supplementary Table 2). Organoids from breast tumor tissue were generated by digesting cells for 1 h in collagenase and organoids from metastatic pleural effusions were generated by isolating tumor spheroids by centrifugation before, in both cases, embedding cancer cells in organoid culture using established protocols that enable long-term propagation of tumor organoids⁶⁶. In parallel, primary human adipocytes were isolated from human breast tissue using an established protocol⁶⁷. For the triple-negative breast cancer organoids derived from primary tumors, we used two different cases, including one in which we generated organoids and isolated mammary gland adipose tissue from the same individual (TOR41). Adipocytes were infected with dCas9–VP64 only (negative control) or *UCP1*-CRISPRa AAV9. After 5 days, they showed strong *mCherry* expression, a fluorescent marker that is part of the gRNA AAV9 (Extended Data Fig. 5a), suggesting that they can be readily infected by our AAVs. In addition, gene analysis showed that both *mCherry* and *UCP1* expression levels were significantly higher in the *UCP1*-CRISPRa-treated adipose organoids than in the control organoids (Extended Data Fig. 5b). Owing to the limited amount of obtainable dissected tissues, we measured glucose and fatty acid uptake of adipocytes isolated from one sample for which we had more abundant material (TOR40). Upon insulin treatment, we found that *UCP1*-CRISPRa-modulated mammary gland adipocytes exhibited increased glucose and fatty acid uptake compared to dCas9–VP64-treated adipocytes (Extended Data Fig. 5c).

To test whether *UCP1*-CRISPRa AAV9 adipocytes can suppress cancer growth, we added them to a hydrogel dome on top of the breast cancer organoids with a fully defined organoid medium⁶⁶ and co-cultured for 5 days (Fig. 5a). In all five cases, we observed a significant reduction in cancer organoid size and, in most organoids, also a reduction in organoid number (TOR124 and TOR41 were not significant) upon incubation with adipocytes infected with *UCP1*-CRISPRa AAV9 compared to the dCas9–VP64-only treated cells (Fig. 5b and Extended Data Fig. 5d). All five cancer organoid cases co-cultured with *UCP1*-CRISPRa had significantly lower proliferation marker *MKI67*

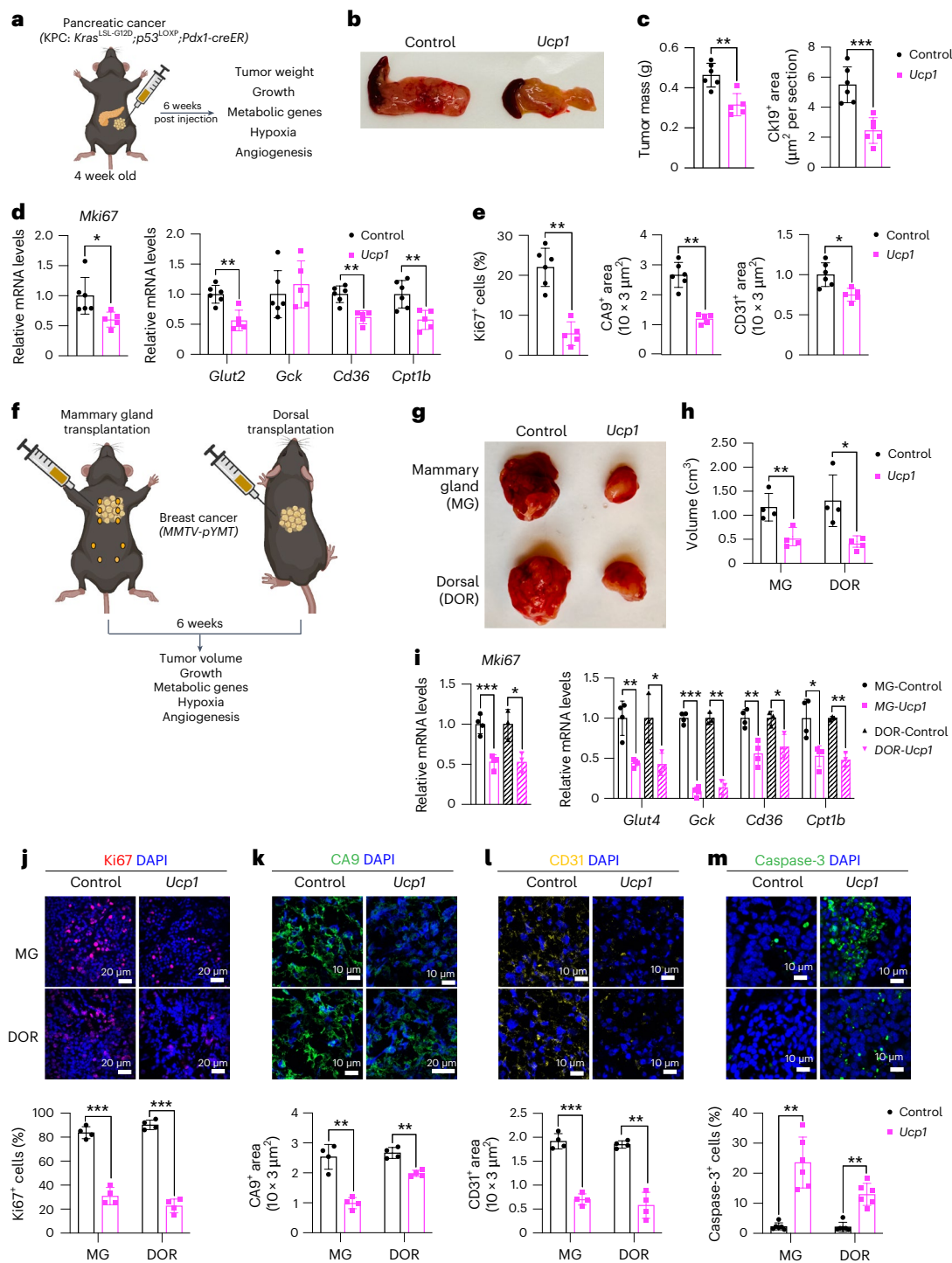


Fig. 4 | Implantation of *Ucp1*-CRISPRa adipose organoids in pancreatic and breast cancer genetic mouse models suppresses cancer development.

a, Schematic of the transplantation model for *Ucp1*-CRISPRa-treated mouse adipose organoids in KPC pancreatic cancer mice and their subsequent phenotyping (created with BioRender.com). **b**, Representative images of the pancreas implanted with *Ucp1*-CRISPRa or control (dCas9-VP64 only) mouse adipose organoids ($n = 5\text{--}6$ mice per treatment). **c**, Mass and immunofluorescence staining of Ck19 (μm^2 per section) of the pancreas transplanted with *Ucp1*-CRISPRa-modulated mouse adipose organoids compared to control (dCas9-VP64 only) ($n = 5\text{--}6$ mice). **d**, RT-qPCR of the proliferation marker gene *Mki67* and metabolic genes *Glut2*, *Gck*, *Cd36* and *Cpt1b* from pancreatic tumors co-transplanted with *Ucp1*-CRISPRa-modulated adipocytes ($n = 5\text{--}6$ biological replicates). **e**, Immunofluorescence quantification of Ki67, CA9 and CD31 in cryosections of tumors ($n = 5\text{--}6$ sections per treatment). **f**, Schematic of the transplantation model for *Ucp1*-CRISPRa-treated mouse adipose organoids in MMTV-pYMT breast cancer mice and their subsequent phenotyping (created with BioRender.com). **g**, Representative images of the breast tumors that were implanted with *Ucp1*-CRISPRa or control (dCas9-VP64 only) adipose organoids in the mammary gland or on the back of the mice (dorsal) ($n = 4$ mice per treatment). **h**, Volume of the tumors transplanted with *Ucp1*-CRISPRa adipose organoids compared to control (dCas9-VP64 only) ($n = 4$ mice). **i**, RT-qPCR of the proliferation marker gene *Mki67* and metabolic genes *Glut4*, *Gck*, *Cd36* and *Cpt1b* from breast tumors co-transplanted with *Ucp1*-CRISPRa-modulated adipocytes ($n = 3\text{--}4$ biological replicates). **j-m**, Immunofluorescence staining and quantification of Ki67 (j), CA9 (k), CD31 (l) and caspase-3 (m) in tumor cryosections ($n = 4\text{--}5$ sections per treatment). White scale bars on the bottom right represent 10 μm (CA9, CD31, caspase 3) or 20 μm (Ki67 and CA9 DOR-*Ucp1*). All statistical tests were carried out using a two-tailed t-test and data are represented as mean \pm s.d. * $P \leq 0.05$; ** $P \leq 0.01$; *** $P \leq 0.001$.

adipose organoids in the mammary gland or on the back of MMTV-PyMT breast cancer mice and their subsequent phenotyping (created with BioRender.com). **g**, Representative images of the breast tumors that were implanted with *Ucp1*-CRISPRa or control (dCas9-VP64 only) adipose organoids in the mammary gland or on the back of the mice (dorsal) ($n = 4$ mice per treatment). **h**, Volume of the tumors transplanted with *Ucp1*-CRISPRa adipose organoids compared to control (dCas9-VP64 only) ($n = 4$ mice). **i**, RT-qPCR of the proliferation marker gene *Mki67* and metabolic genes *Glut4*, *Gck*, *Cd36* and *Cpt1b* from breast tumors co-transplanted with *Ucp1*-CRISPRa-modulated adipocytes ($n = 3\text{--}4$ biological replicates). **j-m**, Immunofluorescence staining and quantification of Ki67 (j), CA9 (k), CD31 (l) and caspase-3 (m) in tumor cryosections ($n = 4\text{--}5$ sections per treatment). White scale bars on the bottom right represent 10 μm (CA9, CD31, caspase 3) or 20 μm (Ki67 and CA9 DOR-*Ucp1*). All statistical tests were carried out using a two-tailed t-test and data are represented as mean \pm s.d. * $P \leq 0.05$; ** $P \leq 0.01$; *** $P \leq 0.001$.

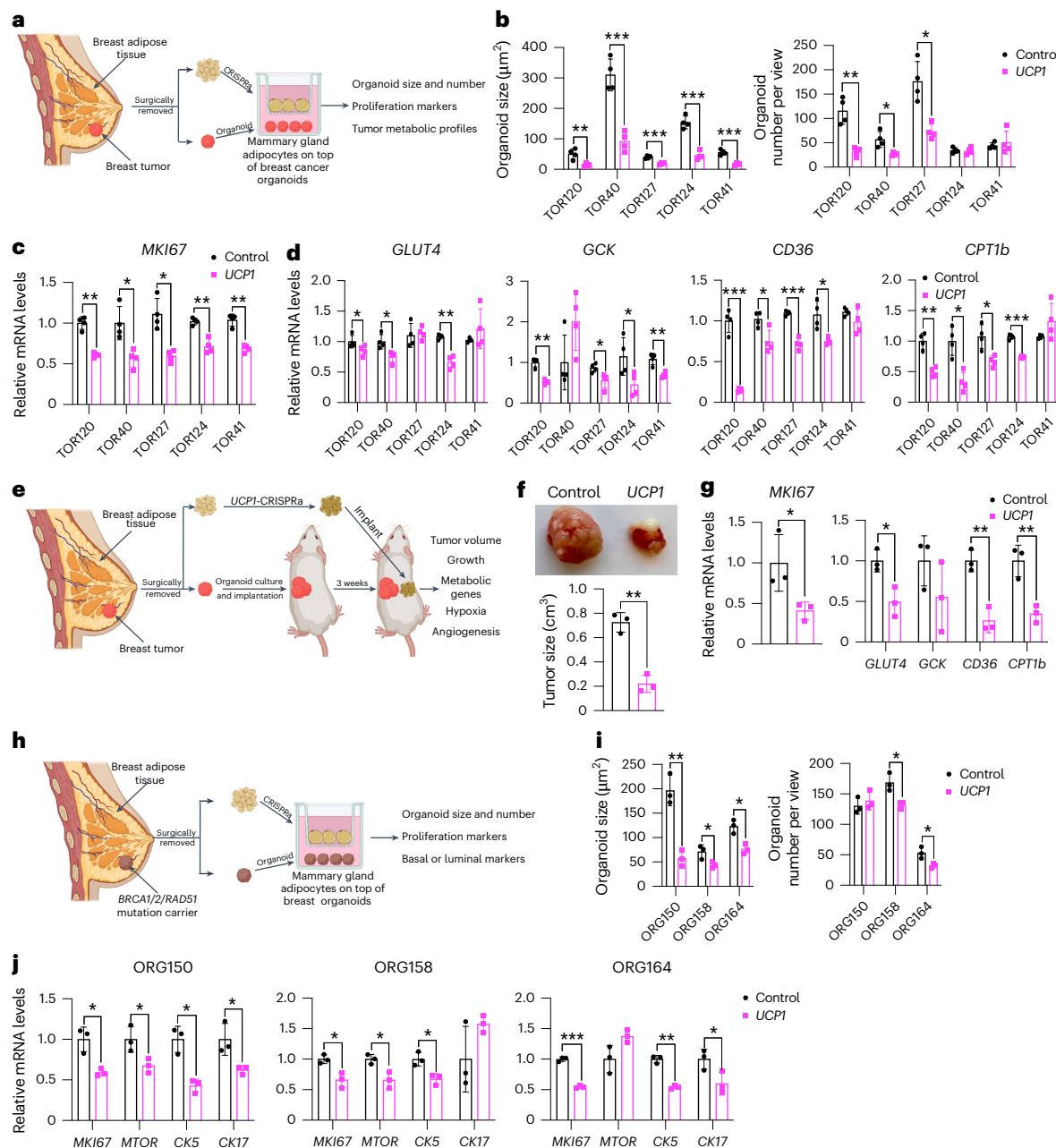


Fig. 5 | Cancer organoids co-cultured with UCP1-CRISPRa adipocytes, both from dissected breast tissue, lead to tumor suppression and prevent cancer development. **a**, Schematic of the co-culturing model of UCP1-CRISPRa-modulated human mammary adipocytes and breast cancer organoids from dissected breast tumors (created with BioRender.com). **b**, Cancer organoid size and numbers of breast tumor organoids from five dissected breast tumors that were co-cultured with UCP1-CRISPRa adipocytes or control (dCas9-VP64 only) adipocytes ($n = 4$ biological replicates). **c,d**, RT-qPCR of the proliferation marker gene MKI67 (c) and metabolic genes GLUT4, GCK, CD36 and CPT1b (d) of breast cancer organoids that were co-cultured with CRISPRa-modulated adipocytes ($n = 4$ biological replicates). **e**, Schematic of the co-transplantation model for breast cancer organoids and UCP1-CRISPRa-treated breast adipocytes in immune-deficient SCID mice and their subsequent phenotyping (created with BioRender.com). **f**, Representative images and tumor size of breast cancer organoids co-implanted with UCP1-CRISPRa or control (dCas9-VP64 only) breast

adipocytes ($n = 3$ biological replicates). **g**, RT-qPCR of the proliferation marker gene MKI67 and metabolic genes GLUT4, GCK, CD36 and CPT1b of breast cancer organoids that were co-cultured with UCP1-CRISPRa or dCas9-VP64-treated breast adipocytes ($n = 3$ biological replicates). **h**, Schematic of the co-culturing model of UCP1-CRISPRa-modulated human mammary adipocytes and breast organoids cultured from breast tissues of BRCA1/BRCA2/RAD51D mutation carriers (created with BioRender.com). **i**, Organoid size and numbers of breast organoids from three resected breast tissues that were co-cultured with UCP1-CRISPRa adipocytes or control (dCas9-VP64 only) adipocytes ($n = 3$ biological replicates). **j**, RT-qPCR of the proliferation marker genes MKI67 and MTOR and CK5 and CK17 of breast organoids that were co-cultured with CRISPRa-modulated adipocytes ($n = 3$ biological replicates). All statistical tests were carried out using a two-tailed *t*-test and data are represented as mean \pm s.d. * $P \leq 0.05$; ** $P \leq 0.01$; *** $P \leq 0.001$.

expression compared to the negative control (Fig. 5c). We also observed significantly decreased levels of GLUT4, GCK, CD36 and CPT1b for most of the UCP1-CRISPRa co-cultured cancer organoids (Fig. 5d), suggesting that they have lower glycolysis and fatty acid metabolism.

We next tested whether UCP1-CRISPRa primary breast adipocytes can suppress breast cancer growth in vivo. We implanted triple-negative breast cancer organoids derived from resected breast tumor into SCID mice for 3 weeks. We used the floating fraction of

mature adipocytes in breast tissue. The cells were cultured, treated with *UCP1*-CRISPRa and mixed with Matrigel before their co-implantation for 3 weeks into mice with tumors (Fig. 5e). After 3 weeks, the tumors were dissected and examined. We found that tumors co-implanted with *UCP1*-CRISPRa adipocytes were significantly smaller than those co-implanted with dCas9–VP64-treated adipocytes (Fig. 5f). In addition, tumors co-implanted with *UCP1*-CRISPRa adipocytes had lower expression of *MKI67*, glycolytic genes (*GLUT4* and *GCK*) and FAO genes (*CD36* and *CPT1b*) (Fig. 5g). Overall, our results demonstrate that human adipocytes from dissected breast tissue can upregulate *UCP1* via AAV9-CRISPRa and are able to reduce glycolysis and fatty acid metabolism and suppress breast cancer organoid growth, both in cell culture and xenografts. Furthermore, this work demonstrates the potential clinical utility of an ex vivo autologous transplantation of CRISPRa-modulated adipocytes to treat cancer.

AMT suppresses high breast cancer risk cell proliferation

To examine whether *UCP1*-CRISPRa mammary adipocytes might prevent cancer development in individuals at high lifetime risk of cancer, we co-cultured them alongside breast organoids from dissected patient-matched breast tissue of *BRCA1*/*BRCA2*/*RADS1D* mutation carriers (Fig. 5h). We obtained three samples dissected from individual donors carrying a *BRCA1* mutation (ORG158), a *BRCA2* mutation (ORG150) and a *RADS1D* mutation (ORG164) (details of specific mutations and patient history in Supplementary Table 2). In all three cases, we observed that breast organoids co-cultured with donor-matched *UCP1*-CRISPRa adipocytes were significantly smaller and had lower organoid numbers (other than ORG150) than in the negative control (Fig. 5i). In addition, we found that *BRCA1*/*BRCA2* breast organoids co-cultured with *UCP1*-CRISPRa adipose organoids had lower expression levels of known proliferation markers *MKI67* and *MTOR* than that of controls (Fig. 5j). Furthermore, these breast organoids exhibited reduced expression levels of *CK5* and *CK17* (other than ORG158) suggesting reduced basal-luminal phenotypes in these *BRCA1*/*BRCA2*/*RADS1D*-heterozygous luminal progenitor-predominant breast cells^{68,69} (Fig. 5j). In summary, our results suggest that *UCP1*-CRISPRa breast adipocytes may inhibit premalignant phenotypes in breast organoids from donors with inherited cancer predisposition syndromes.

Inducible or cell-scaffold AMT suppresses cancer progression

To further enhance the translation capabilities of AMT, we developed inducible AAV vectors designed to turn on dCas9–VP64 upon tetracycline treatment, thereby enabling tight regulation of *UCP1* gene expression in adipocytes or adipose organoids. We cloned the reverse tetracycline-control transactivator (rtTA) downstream of the CMV promoter into the gRNA-AAV vector and the tetracycline response element (TRE) and a minimal promoter upstream of dCas9–VP64 in

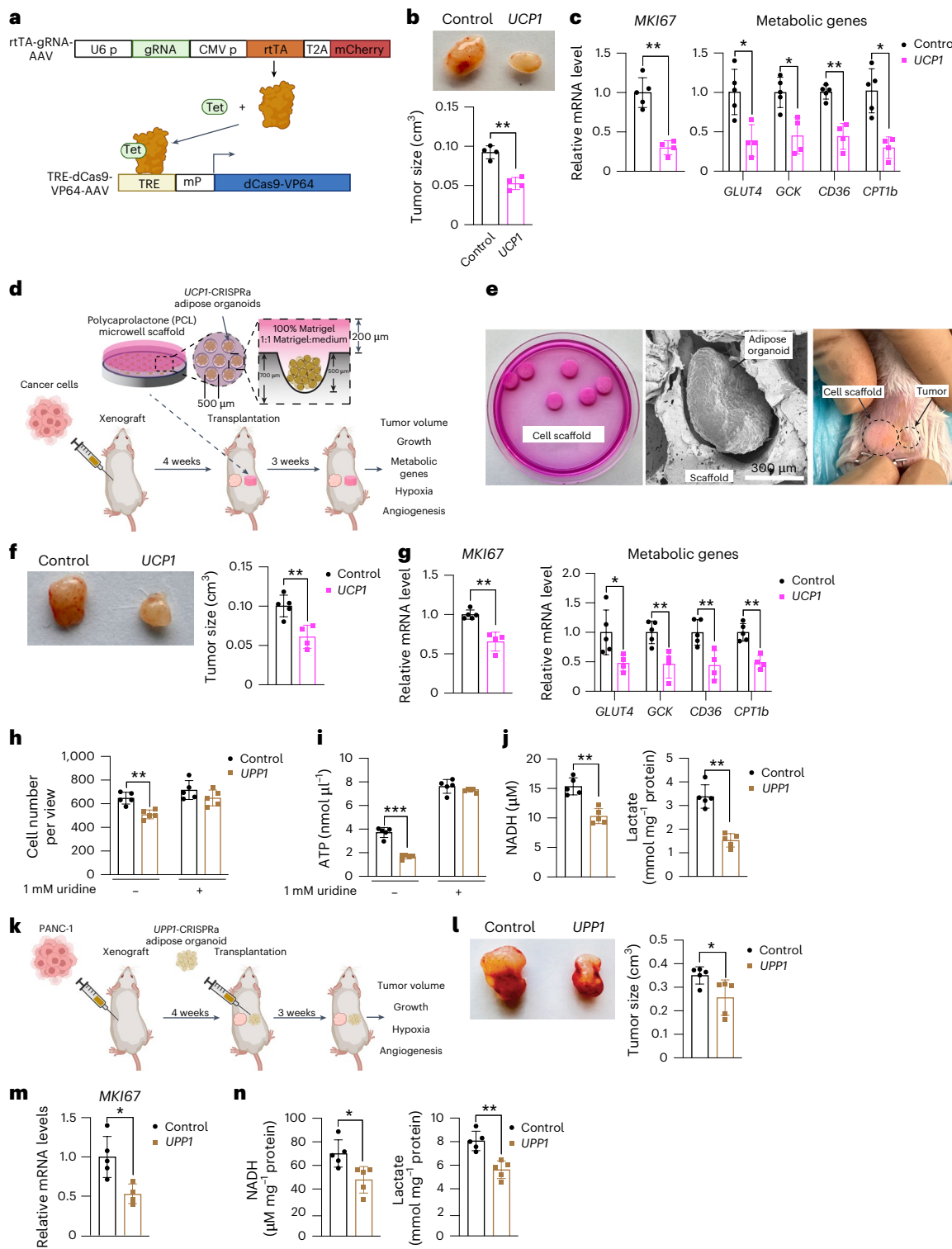
the dCas9–VP64 AAV vector. Upon tetracycline treatment, rtTA binds to TRE and induces dCas9–VP64 expression. b, Representative image and tumor size of MCF-7 tumors that were co-implanted with *UCP1*-CRISPRa or control (dCas9–VP64 only) human adipose organoids ($n = 4$ biological replicates). c, RT-qPCR of proliferation marker gene *MKI67* and metabolic genes (*GLUT4*, *GCK*, *CD36* and *CPT1b*) of tumors co-implanted with CRISPRa-modulated adipocytes ($n = 4$ –5 biological replicates). d, Schematic of co-transplantation of MCF-7 tumors and cell scaffolds containing *UCP1*-CRISPRa or control (dCas9–VP64 only) human adipose organoids and tumor phenotyping (lower panel created with BioRender.com). e, Representative images of cell scaffolds in plate (left), electron microscopy image (1.0 kV, $\times 500$ and 7.895 mm lens) of scaffold containing an adipose organoid (middle) and the scaffold implanted in mice (right). f, Representative image and tumor size of MCF-7 tumors co-implanted with cell scaffold containing *UCP1*-CRISPRa or control (dCas9–VP64 only) human adipose organoids ($n = 4$ –5 biological replicates). g, RT-qPCR of the proliferation marker gene *MKI67* and metabolic genes (*GLUT4*, *GCK*, *CD36* and *CPT1b*) of tumors co-implanted with CRISPRa-modulated adipocytes ($n = 4$ –5 biological replicates). h, Cell number per view of PANC-1 pancreatic cancer cells that were co-cultured with *UPP1*-CRISPRa or control (dCas9–VP64 only) human adipocytes in media without (–) or with (+) 1 mM uridine ($n = 5$ biological replicates). i, ATP levels measured in PANC-1 pancreatic cancer cells co-cultured with *UPP1*-CRISPRa-modulated adipocytes without (–) or with (+) excess uridine ($n = 5$ biological replicates). j, NADH and lactate levels in PANC-1 pancreatic cancer cells that were co-cultured with *UPP1*-CRISPRa-modulated adipocytes without the addition of uridine ($n = 5$ biological replicates). k, Schematic of the co-transplantation of PANC-1 tumors with *UPP1*-CRISPRa-modulated adipose organoid in SCID mice. l, Representative image and size of PANC-1 xenograft tumor co-implanted with dCas9–VP64 or *UPP1*-CRISPRa-modulated adipose organoids ($n = 5$ biological replicates). m, RT-qPCR of *MKI67*. n, NADH and lactate levels in PANC-1 tumors that were co-implanted with dCas9–VP64 or *UPP1*-CRISPRa-modulated adipose organoids ($n = 5$ biological replicates). All statistical tests were carried out using a two-tailed *t*-test and data are represented as mean \pm s.d. * $P \leq 0.05$; ** $P \leq 0.01$; *** $P \leq 0.001$.

Fig. 6 | Development of inducible AMT systems and the use of AMT to upregulate *UPP1* to suppress PDA. a, Schematic of the inducible CRISPRa-AAV system (created with BioRender.com). Upon tetracycline treatment, rtTA binds to TRE and induces dCas9–VP64 expression. **b**, Representative image and tumor size of MCF-7 tumors that were co-implanted with *UCP1*-CRISPRa or control (dCas9–VP64 only) human adipose organoids ($n = 4$ biological replicates). **c**, RT-qPCR of proliferation marker gene *MKI67* and metabolic genes (*GLUT4*, *GCK*, *CD36* and *CPT1b*) of tumors co-implanted with CRISPRa-modulated adipocytes ($n = 4$ –5 biological replicates). **d**, Schematic of co-transplantation of MCF-7 tumors and cell scaffolds containing *UCP1*-CRISPRa or control (dCas9–VP64 only) human adipose organoids and tumor phenotyping (lower panel created with BioRender.com). **e**, Representative images of cell scaffolds in plate (left), electron microscopy image (1.0 kV, $\times 500$ and 7.895 mm lens) of scaffold containing an adipose organoid (middle) and the scaffold implanted in mice (right). **f**, Representative image and tumor size of MCF-7 tumors co-implanted with cell scaffold containing *UCP1*-CRISPRa or control (dCas9–VP64 only) human adipose organoids ($n = 4$ –5 biological replicates). **g**, RT-qPCR of the proliferation marker gene *MKI67* and metabolic genes (*GLUT4*, *GCK*, *CD36* and *CPT1b*) of tumors co-implanted with CRISPRa-modulated adipocytes ($n = 4$ –5 biological replicates). **h**, Cell number per view of PANC-1 pancreatic cancer cells that were co-cultured with *UPP1*-CRISPRa or control (dCas9–VP64 only) human adipocytes in media without (–) or with (+) 1 mM uridine ($n = 5$ biological replicates). **i**, ATP levels measured in PANC-1 pancreatic cancer cells co-cultured with *UPP1*-CRISPRa-modulated adipocytes without (–) or with (+) excess uridine ($n = 5$ biological replicates). **j**, NADH and lactate levels in PANC-1 pancreatic cancer cells that were co-cultured with *UPP1*-CRISPRa-modulated adipocytes without the addition of uridine ($n = 5$ biological replicates). **k**, Schematic of the co-transplantation of PANC-1 tumors with *UPP1*-CRISPRa-modulated adipose organoid in SCID mice. **l**, Representative image and size of PANC-1 xenograft tumor co-implanted with dCas9–VP64 or *UPP1*-CRISPRa-modulated adipose organoids ($n = 5$ biological replicates). **m**, RT-qPCR of *MKI67*. **n**, NADH and lactate levels in PANC-1 tumors that were co-implanted with dCas9–VP64 or *UPP1*-CRISPRa-modulated adipose organoids ($n = 5$ biological replicates). All statistical tests were carried out using a two-tailed *t*-test and data are represented as mean \pm s.d. * $P \leq 0.05$; ** $P \leq 0.01$; *** $P \leq 0.001$.

Uridine-based AMT suppresses PDA

To examine whether AMT can be used to treat other cancer-associated metabolic pathways, we upregulated the uridine phosphorylase 1 (*UPP1*) gene in human adipocytes and adipose organoids and tested whether they can suppress PDA, which is known to use uridine-derived ribose in glucose-restricted conditions³⁵. Using CRISPRick³⁶, we designed five gRNAs to upregulate *UPP1* gene expression in human adipocytes and found that all gRNAs were able to induce *UPP1* expression in these cells (Extended Data Fig. 6c). We next generated an AAV9 virus for two gRNAs and transduced human adipocytes with AAV9, finding that both

gRNAs significantly induced *UPP1* gene expression (Extended Data Fig. 6c). We used the top-activating gRNA AAV for all subsequent experiments. We next transduced human adipocytes with *UPP1*-CRISPRa AAV9 and incubated these cells with ³H-labelled uridine. We found these adipocytes to significantly uptake uridine during a 12-h incubation (Extended Data Fig. 6d) and have increased lactate levels, a byproduct of uridine catabolism (Extended Data Fig. 6e). We next co-cultured a PDA cell line, PANC-1, with *UPP1*-CRISPRa or dCas9-VP64 only (negative control) human adipocytes on top of Transwell plates. Cells were cultured in low-glucose-containing media with or without an excess



amount of uridine. We found that PANC-1 cells that were co-cultured with the *UPP1*-CRISPRa adipocytes had a significantly lower number of cells than those co-cultured with dCas9–VP64 adipocytes (Fig. 6h). This growth suppression was abolished with the addition of uridine (Fig. 6h). PANC-1 cells that were co-cultured with *UPP1*-CRISPRa adipocytes had lower ATP levels than control PANC-1 cells. By contrast, with an excess amount of uridine, there was no apparent difference in ATP levels between PANC-1 cells with *UPP1*-CRISPRa adipocytes and control cells (Fig. 6i). Furthermore, PANC-1 cells that were co-cultured with *UPP1*-CRISPRa-modulated adipocytes had lower NADH and lactate levels than control cells (Fig. 6j). We next carried out a similar study but grew the cells in a high-glucose-containing media and found that the growth suppression of PANC-1 by *UPP1*-CRISPRa adipocytes was reduced (Extended Data Fig. 6f). Combined, these assays suggest that *UPP1*-CRISPRa adipocytes have increased uridine use and can outcompete PDA for uridine use in low-glucose conditions.

We next set out to test whether *UPP1*-CRISPRa can suppress PDA xenograft growth. We implanted PANC-1 cells in SCID mice for 4 weeks, followed by the implantation of *UPP1*-CRISPRa and dCas9–VP64 only (negative control) adipose organoids (Fig. 6k). After 3 weeks, tumors were dissected and examined. We found that tumors co-implanted with *UPP1*-CRISPRa human adipose organoids were significantly smaller than those co-implanted with dCas9–VP64 adipose organoids (Fig. 6l). In addition, these tumors had lower expression of the proliferation marker *MKI67* (Fig. 6m). All the byproducts of uridine catabolism, including NADH and lactate, were found to be significantly reduced in tumors co-implanted with *UPP1*-CRISPRa human adipose organoids (Fig. 6n). In summary, these results suggest that CRISPRa upregulation of *UPP1* in adipocytes and adipose organoids reduces uridine in the tumor microenvironment of PDA and leads to cancer growth suppression. These results also demonstrate the clinical versatility and capacity of AMT to target various cancer metabolic pathways.

Discussion

Cancer cells are fast-proliferating cells that require large amounts of nutrients, including glucose and fatty acids. They can reprogram metabolic pathways to use available substrates in the surrounding environment. Targeting their metabolism can be a potent cancer treatment. Here, we developed a cell-based cancer therapeutic approach that uses modified adipocytes to target various cancer metabolic pathways and has the potential to treat a wide variety of cancers. Adipocytes offer a unique ex vivo therapeutic system, with many of the needed procedures already established in the clinic. Liposuction and fat transplantation are commonly used in many surgical procedures, such as aesthetic and reconstructive surgery. Owing to successful engraftment, adipose tissue transplantation has progressively evolved, not only in plastic and reconstructive surgery but also for therapeutic treatments⁸⁰. Several reports using rodent models have shown that BAT transplantation has beneficial metabolic outcomes^{81–84}. These also include the use of *UCP1*-CRISPRa modulation in human white preadipocytes to induce browning, followed by their transplantation in mice on a HFD, leading to improved body weight, glucose tolerance and insulin sensitivity³⁴. Our work showcases how these ‘brown’ adipocytes and adipose organoids can be used for cancer treatment. In addition, given that adipocytes are ‘metabolic engines’, they can also be engineered to outcompete tumors that use various metabolic pathways, as we show for PDA. Adipocytes are also extensive secretors⁸⁵, and AMT could be used to secrete tumor-targeting factors. The use of cell scaffolds, as done here, could be leveraged by removing and replacing cell scaffolds that contain adipose organoids that target different cancer metabolic pathways, further ‘personalizing’ this therapeutic approach.

There is a growing interest in implementing human adipose tissue grafting by using adipose stem cells or progenitors because of their resistance to trauma and long-term survival following transplantation.

One such example is the use of CRISPRa to upregulate the relaxin family peptide receptor 1 (*RXFP1*) gene in adipose-derived stem cells and their transplantation in a diabetes mellitus-induced erectile dysfunction rat model, showing amelioration of the erectile dysfunction phenotype⁸⁶. Organoids could be advantageous for these cells, as they provide a 3D culture that can better recapitulate the heterogeneity of adipose tissue, respond better to endogenous stimuli and form tissue micro-environments that could more efficiently integrate with cancer cells following transplantation. Several groups have successfully grown adipose organoids from mouse adipose stem cells^{33,48,49,87}. Here, we were able to culture human adipose organoids from preadipocytes using various conditions from previous studies^{33,48,49,87}. These human adipose organoids exhibited mature adipocyte markers, including *FABP4* and *PLIN1*. Finally, in our study, we show that the CRISPRa modulation can significantly reduce tumor size, glycolysis, fatty acid metabolism and uridine use and improve hypoxia and angiogenesis in cancer mouse models. Further development of these organoids and their modulation as well as determination of the number of cells needed to achieve a therapeutic benefit could improve these attributes and their therapeutic use for a wide range of diseases.

Our work builds on the recent observation that activating BAT through cold exposure increases adipocyte glucose uptake and lipid metabolism and significantly inhibits tumor progression¹⁵. Here, instead of placing tumor models in cold conditions, we took advantage of CRISPRa to increase the gene expression of key BAT regulators, including *UCP1*, *PPARGC1A* and *PRDM16*, to engineer adipocytes to have increased glucose and fatty acid uptake and metabolism and then used them to deplete resources from cancer cells. Similar to the BAT cold activation studies¹⁵, we observed that high glucose feeding mitigates cancer suppression. In addition, we show that MCF-7 xenograft mice on a HFD have reduced cancer suppression, suggesting that fatty acid competition is also involved in this mechanism. Implanting CRISPRa-modulated adipose organoids distal to the tumors also led to suppression of cancer growth, suggesting that resource competition, similar to BAT cold activation studies¹⁵, can be carried out distal to the tumor and that complex surgical implantation procedures for tumors with limited access might not be needed for AMT. The observed tumor suppression could also be a result of additional mechanisms. The CRISPRa-modulated adipose organoids could modulate whole-body metabolism. Previous studies have shown that hyperinsulinemia can lead to cancer growth due to insulin being a powerful mitogen and survival factor^{88–90}. For example, the administration of dapagliflozin, an SGLT2 inhibitor that lowers blood glucose, and a controlled-release mitochondrial protonophore (CRMP) suppresses cancer growth in mice by reversing hyperinsulinemia⁹¹. Given that BAT is widely known to reduce whole-body blood glucose and insulin levels in humans^{15,83,92}, we reason that the CRISPRa-modulated adipose organoids could also reduce cancer progression by lowering plasma insulin levels. Indeed, our data, using both xenograft and genetic mouse models, show that mice implanted with CRISPRa-modulated adipose organoids exhibit reduced plasma insulin levels compared to the dCas9–VP64 control mice (Extended Data Figs. 3c and 4g,i).

Among BAT-activating genes, *UCP1* showed the most robust effect in terms of cancer suppression. It would be interesting to further develop this AMT approach to upregulate additional genes that could aid in cancer therapy. These could include, for example, upregulation of *GLUT1* and *GLUT4*, which are the main glucose transporters in adipose cells, with *GLUT4* being the most abundant and insulin-responsive⁹³; glucose-metabolism-associated genes, such as the transcription factor *FOXO1* (ref. 94) and the G-protein coupled receptors *GPR40* and *GPR120*, which have been implicated in improved glucose uptake and insulin resistance^{95,96}; *AIFM2*, which promotes glycolysis in BAT⁹⁷; and FAO-associated genes, including, for example, the fatty acid transporter *CD36*, a key transporter for FAO, *CPT1b* and the fatty acid breakdown enzyme, *ACCI*. Finally, as shown in our study with *UPP1*-CRISPRa

and PDA, AMT can be customized to fit different cancer metabolic programs. Additional modifications could also be engineered in these adipocytes and adipose organoids, including the use of their endocrine capabilities⁹⁸ to secrete chemotherapeutic drugs or other cancer therapeutic-associated compounds or take advantage of their extracellular vesicles, which are known to have an important role in metabolic regulation⁹⁹. AMT could also be readily implemented with various cancer treatments (surgery, drugs, chemotherapy, radiation and others) that, combined, will increase therapeutic impact.

In this study, we used AAV-based CRISPRa to upregulate genes. CRISPRa has several advantages, including tight regulation owing to the use of the endogenous regulatory machinery¹⁰⁰ and the ability to simultaneously upregulate multiple genes. However, it is worth noting that both upregulation and delivery could also be carried out using other modalities. For example, gene upregulation could be carried out using zinc fingers, TALENs, generation of specific mutations using regular CRISPR editing or base or prime editing in promoters or enhancers, or standard overexpression using a cDNA mammalian expression construct of the gene of interest. Adipocytes could also be ‘browned’ using various differentiation cocktails¹⁰¹, cold activation¹⁰² or drugs, such as β 3 agonists^{102,103}, which could also be used to achieve higher competition for nutrients. In addition, various drugs could be used to induce different metabolic pathways. Delivery could be carried out with other viruses, such as lentiviruses that are widely used for chimeric antigen receptor (CAR)-T cell therapy but have a major caveat of genomic integration, or various non-viral nucleic acid delivery vehicles such as nanoparticles¹⁰⁴ or virus-like particles¹⁰⁵. Various drugs could also be used to upregulate specific genes in adipocytes in a global manner in cancer patients. In addition, the downregulation of certain genes in adipocytes or adipose organoids using CRISPR inactivation (CRISPRi), short interfering RNA, CRISPR editing or other techniques could also be used for AMT. For example, a recent study used CRISPR to deplete the nuclear receptor interacting protein 1 (*NRIP1*) gene to make ‘brown’ adipocytes that, upon implantation, decreased the adiposity of mice on a HFD¹⁰⁶.

A link between obesity, excess amount of WAT and cancer development and progression has been established, with nearly 40% of all cancer deaths in the United States being attributed to obesity¹⁰⁷. There have been numerous mechanisms proposed to explain how WAT is linked to cancer development and progression, including chronic inflammation, hyperinsulinemia, steroid hormones and adipokines^{108–114}. In addition, in glucose-rich conditions, cancer cells synthesize de novo fatty acids from intermediates of the glycolysis–TCA cycle (lipogenesis)^{115,116}. The synthesized fatty acids are then used to synthesize triglycerides and are stored as lipid droplets in cancer cells. When energy is needed, these lipid droplets undergo lipolysis to release fatty acids, which are subjected to β -oxidation^{116–118}. Given that BAT is highly associated with improved glucose tolerance and insulin sensitivity¹¹⁹, one could envision a personalized treatment developed for patients with cancer and obesity, whereby AMT is used not only to target cancer and its unique metabolism but also to treat the patients’ metabolic disease. One major hurdle in our approach that needs to be taken into account is cancer-associated cachexia⁵⁰. Although we did not observe weight loss in our mouse models, a longer treatment time could potentially lead to a reduction in body weight, as was shown for *UCP1*-CRISPRa mice on a HFD³⁴. Having the ability to control transgene expression in the modified adipocytes and adipose organoids using drugs (such as tetracycline used in our assays) or the ability to remove these cells with the use of an integrated cell-scaffold delivery platform (as also done in our study) could allow the use of this therapeutic approach in a tightly regulated and reversible manner^{120–125}. This potential to turn therapeutic intervention on and off holds the key to effectively addressing concerns regarding unforeseen clinical complications, adverse outcomes, changing patient conditions or emerging developments in treatment regimens or tumor metabolic pathways.

In summary, our results provide proof-of-principle results for a cancer therapeutic approach, termed AMT, that can be further developed and personalized for specific cancers and patients. Similar to CAR-T cell therapy, AMT can be readily used in the clinic because cells can be obtained from cancer patients through liposuction or other procedures, engineered and transplanted back into the same individual for therapeutic benefit. The use of adipocytes from dissected breast tissue, as performed in our study, further showcases the clinical utility of such an ex vivo approach. In particular, this could be particularly straightforward for breast cancer, as many mastectomies are followed up by reconstructive surgery with autologous tissue¹²⁶, which could be manipulated before this procedure. Unlike T cells, adipocytes have a lower immune response^{34,127}, which could allow more straightforward development of ‘off-the-shelf’ adipocytes or adipose organoids for cancer and other treatments. Their ease of growth in culture, longevity, robustness, lower multiplicity¹²⁸ and endocrine capabilities, along with existing clinical procedures for removal and transplantation, make them a beneficial cell type for cancer and other cellular-based disease therapies.

Online content

Any methods, additional references, Nature Portfolio reporting summaries, source data, extended data, supplementary information, acknowledgements, peer review information; details of author contributions and competing interests; and statements of data and code availability are available at <https://doi.org/10.1038/s41587-024-02551-2>.

References

1. Lin, X., Xiao, Z., Chen, T., Liang, S. H. & Guo, H. Glucose metabolism on tumor plasticity, diagnosis, and treatment. *Front. Oncol.* **10**, 317 (2020).
2. Hay, N. Reprogramming glucose metabolism in cancer: Can it be exploited for cancer therapy? *Nat. Rev. Cancer* **16**, 635–649 (2016).
3. Liberti, M. V. & Locasale, J. W. The Warburg effect: How does it benefit cancer cells? *Trends Biochem. Sci.* **41**, 211–218 (2016).
4. Nagarajan, S. R., Butler, L. M. & Hoy, A. J. The diversity and breadth of cancer cell fatty acid metabolism. *Cancer Metab.* **9**, 2 (2021).
5. Palm, W. & Thompson, C. B. Nutrient acquisition strategies of mammalian cells. *Nature* **546**, 234–242 (2017).
6. DeWaal, D. et al. Hexokinase-2 depletion inhibits glycolysis and induces oxidative phosphorylation in hepatocellular carcinoma and sensitizes to metformin. *Nat. Commun.* **9**, 446 (2018).
7. Chan, D. A. et al. Targeting GLUT1 and the Warburg effect in renal cell carcinoma by chemical synthetic lethality. *Sci. Transl. Med.* **3**, 94ra70 (2011).
8. Liu, Y. et al. A small-molecule inhibitor of glucose transporter 1 downregulates glycolysis, induces cell-cycle arrest, and inhibits cancer cell growth in vitro and in vivo. *Mol. Cancer Ther.* **11**, 1672–1682 (2012).
9. Fernandez, L. P., Gomez de Cedron, M. & Ramirez de Molina, A. Alterations of lipid metabolism in cancer: implications in prognosis and treatment. *Front. Oncol.* **10**, 577420 (2020).
10. Khan, W. et al. Lipid metabolism in cancer: a systematic review. *J. Carcinog.* **20**, 4 (2021).
11. Wang, W., Bai, L., Li, W. & Cui, J. The lipid metabolic landscape of cancers and new therapeutic perspectives. *Front. Oncol.* **10**, 605154 (2020).
12. Snaebjornsson, M. T., Janaki-Raman, S. & Schulze, A. Greasing the wheels of the cancer machine: the role of lipid metabolism in cancer. *Cell Metab.* **31**, 62–76 (2020).
13. Mason, P. et al. SCD1 inhibition causes cancer cell death by depleting mono-unsaturated fatty acids. *PLoS ONE* **7**, e33823 (2012).

14. Guseva, N. V., Rokhlin, O. W., Glover, R. A. & Cohen, M. B. TOFA (5-tetradecyl-oxy-2-furoic acid) reduces fatty acid synthesis, inhibits expression of AR, neuropilin-1 and Mcl-1 and kills prostate cancer cells independent of p53 status. *Cancer Biol. Ther.* **12**, 80–85 (2011).
15. Seki, T. et al. Brown-fat-mediated tumour suppression by cold-altered global metabolism. *Nature* **608**, 421–428 (2022).
16. Symonds, M. E., Aldiss, P., Pope, M. & Budge, H. Recent advances in our understanding of brown and beige adipose tissue: the good fat that keeps you healthy. *F1000Res* **7**, F1000 (2018).
17. Virtanen, K. A. et al. Functional brown adipose tissue in healthy adults. *N. Engl. J. Med.* **360**, 1518–1525 (2009).
18. Cannon, B. & Nedergaard, J. Brown adipose tissue: function and physiological significance. *Physiol. Rev.* **84**, 277–359 (2004).
19. Klingenberg, M. Uncoupling protein—a useful energy dissipator. *J. Bioenerg. Biomembr.* **31**, 419–430 (1999).
20. Suzuki, D., Murata, Y. & Oda, S. Changes in Ucp1, D2 (Dio2) and Glut4 (*Slc2a4*) mRNA expression in response to short-term cold exposure in the house musk shrew (*Suncus murinus*). *Exp. Anim.* **56**, 279–288 (2007).
21. Vimaleswaran, K. S., Radha, V., Deepa, R. & Mohan, V. Absence of association of metabolic syndrome with PPARGC1A, PPARG and UCP1 gene polymorphisms in Asian Indians. *Metab. Syndr. Relat. Disord.* **5**, 153–162 (2007).
22. Feldmann, H. M., Golozoubova, V., Cannon, B. & Nedergaard, J. UCP1 ablation induces obesity and abolishes diet-induced thermogenesis in mice exempt from thermal stress by living at thermoneutrality. *Cell Metab.* **9**, 203–209 (2009).
23. Tabuchi, C. & Sul, H. S. Corrigendum: signaling pathways regulating thermogenesis. *Front. Endocrinol. (Lausanne)* **12**, 698619 (2021).
24. Yi, D. et al. Zc3h10 acts as a transcription factor and is phosphorylated to activate the thermogenic program. *Cell Rep.* **29**, 2621–2633.e4 (2019).
25. Puigserver, P. & Spiegelman, B. M. Peroxisome proliferator-activated receptor- γ coactivator 1 α (PGC-1 α): transcriptional coactivator and metabolic regulator. *Endocr. Rev.* **24**, 78–90 (2003).
26. Lin, J. et al. Defects in adaptive energy metabolism with CNS-linked hyperactivity in PGC-1 α null mice. *Cell* **119**, 121–135 (2004).
27. Kajimura, S. Promoting brown and beige adipocyte biogenesis through the PRDM16 pathway. *Int. J. Obes. Suppl.* **5**, S11–S14 (2015).
28. Harms, M. J. et al. PRDM16 binds MED1 and controls chromatin architecture to determine a brown fat transcriptional program. *Genes Dev.* **29**, 298–307 (2015).
29. Ohno, H., Shinoda, K., Spiegelman, B. M. & Kajimura, S. PPARgamma agonists induce a white-to-brown fat conversion through stabilization of PRDM16 protein. *Cell Metab.* **15**, 395–404 (2012).
30. Kajimura, S. et al. Initiation of myoblast to brown fat switch by a PRDM16-C/EBP- β transcriptional complex. *Nature* **460**, 1154–1158 (2009).
31. Seale, P. et al. PRDM16 controls a brown fat/skeletal muscle switch. *Nature* **454**, 961–967 (2008).
32. Kajimura, S. et al. Regulation of the brown and white fat gene programs through a PRDM16/CtBP transcriptional complex. *Genes Dev.* **22**, 1397–1409 (2008).
33. Seale, P. et al. Transcriptional control of brown fat determination by PRDM16. *Cell Metab.* **6**, 38–54 (2007).
34. Wang, C. H. et al. CRISPR-engineered human brown-like adipocytes prevent diet-induced obesity and ameliorate metabolic syndrome in mice. *Sci. Transl. Med.* **12**, eaaz8664 (2020).
35. Nwosu, Z. C. et al. Uridine-derived ribose fuels glucose-restricted pancreatic cancer. *Nature* **618**, 151–158 (2023).
36. Kim, H. K. et al. Deep learning improves prediction of CRISPR-Cpf1 guide RNA activity. *Nat. Biotechnol.* **36**, 239–241 (2018).
37. Flint, J. & Shenk, T. Viral transactivating proteins. *Annu. Rev. Genet.* **31**, 177–212 (1997).
38. Wu, Z., Yang, H. & Colosi, P. Effect of genome size on AAV vector packaging. *Mol. Ther.* **18**, 80–86 (2010).
39. Bates, R., Huang, W. & Cao, L. Adipose tissue: an emerging target for adeno-associated viral vectors. *Mol. Ther. Methods Clin. Dev.* **19**, 236–249 (2020).
40. Kaushik, N., Kaushik, N. K., Choi, E. H. & Kim, J. H. Blockade of cellular energy metabolism through 6-aminonicotinamide reduces proliferation of non-small lung cancer cells by inducing endoplasmic reticulum stress. *Biology (Basel)* **10**, 1088 (2021).
41. Li, Y. et al. Targeting glucose-6-phosphate dehydrogenase by 6-AN induces ROS-mediated autophagic cell death in breast cancer. *FEBS J.* **290**, 763–779 (2023).
42. Varshney, R., Dwarakanath, B. & Jain, V. Radiosensitization by 6-aminonicotinamide and 2-deoxy-D-glucose in human cancer cells. *Int. J. Radiat. Biol.* **81**, 397–408 (2005).
43. O'Connor, R. S. et al. The CPT1a inhibitor, etomoxir induces severe oxidative stress at commonly used concentrations. *Sci. Rep.* **8**, 6289 (2018).
44. Shim, J.-K. et al. Etomoxir, a carnitine palmitoyltransferase 1 inhibitor, combined with temozolomide reduces stemness and invasiveness in patient-derived glioblastoma tumorspheres. *Cancer Cell Int.* **22**, 309 (2022).
45. Lee, C.-K. et al. Tumor metastasis to lymph nodes requires YAP-dependent metabolic adaptation. *Science* **363**, 644–649 (2019).
46. Loo, S. Y. et al. Fatty acid oxidation is a druggable gateway regulating cellular plasticity for driving metastasis in breast cancer. *Sci. Adv.* **7**, eabh2443 (2021).
47. Manerba, M. et al. Metabolic activation triggered by cAMP in MCF-7 cells generates lethal vulnerability to combined oxamate/etomoxir. *Biochim. Biophys. Acta Gen. Subj.* **1863**, 1177–1186 (2019).
48. Strobel, H. A., Gerton, G. & Hoyng, J. B. Vascularized adipocyte organoid model using isolated human microvessel fragments. *Biofabrication* **13**, 035022 (2021).
49. Taylor, J. et al. Generation of immune cell containing adipose organoids for in vitro analysis of immune metabolism. *Sci. Rep.* **10**, 21104 (2020).
50. Kir, S. & Spiegelman, B. M. Cachexia and brown fat: a burning issue in cancer. *Trends Cancer* **2**, 461–463 (2016).
51. Bierie, B. et al. Integrin- β 4 identifies cancer stem cell-enriched populations of partially mesenchymal carcinoma cells. *Proc. Natl. Acad. Sci. USA* **114**, E2337–E2346 (2017).
52. Saito, Y. et al. LLGL2 rescues nutrient stress by promoting leucine uptake in ER $^+$ breast cancer. *Nature* **569**, 275–279 (2019).
53. Takaku, M., Grimm, S. A. & Wade, P. A. GATA3 in breast cancer: Tumor suppressor or oncogene? *Gene Expr.* **16**, 163–168 (2015).
54. Jia, L. et al. eEF1A2 interacts with HSP90AB1 to promote lung adenocarcinoma metastasis via enhancing TGF- β /SMAD signalling. *Br. J. Cancer* **124**, 1301–1311 (2021).
55. Giudici, F. et al. Elevated levels of eEF1A2 protein expression in triple negative breast cancer relate with poor prognosis. *PLoS ONE* **14**, e0218030 (2019).
56. Abrahams, A., Parker, M. I. & Prince, S. The T-box transcription factor Tbx2: its role in development and possible implication in cancer. *IUBMB Life* **62**, 92–102 (2010).
57. Yang, H. et al. HOXD10 acts as a tumor-suppressive factor via inhibition of the RHOC/AKT/MAPK pathway in human cholangiocellular carcinoma. *Oncol. Rep.* **34**, 1681–1691 (2015).
58. Chang, J. W. et al. Wild-type p53 upregulates an early onset breast cancer-associated gene GAS7 to suppress metastasis via GAS7-CYFIP1-mediated signaling pathway. *Oncogene* **37**, 4137–4150 (2018).

59. Liu, S. et al. MAP2K4 interacts with Vimentin to activate the PI3K/AKT pathway and promotes breast cancer pathogenesis. *Aging (Albany NY)* **11**, 10697–10710 (2019).
60. Aizawa, T. et al. Cancer-associated fibroblasts secrete Wnt2 to promote cancer progression in colorectal cancer. *Cancer Med.* **8**, 6370–6382 (2019).
61. Joshi, S. et al. Rac2 controls tumor growth, metastasis and M1–M2 macrophage differentiation in vivo. *PLoS ONE* **9**, e95893 (2014).
62. Ashburner, M. et al. Gene ontology: tool for the unification of biology. The Gene Ontology Consortium. *Nat. Genet.* **25**, 25–29 (2000).
63. Gene Ontology Consortium et al. The gene ontology knowledgebase in 2023. *Genetics* **224**, iyad031 (2023).
64. Maddipati, R. & Stanger, B. Z. Pancreatic cancer metastases harbor evidence of polyclonality. *Cancer Discov.* **5**, 1086–1097 (2015).
65. Guy, C. T., Cardiff, R. D. & Muller, W. J. Induction of mammary tumors by expression of polyomavirus middle T oncogene: a transgenic mouse model for metastatic disease. *Mol. Cell. Biol.* **12**, 954–961 (1992).
66. Dekkers, J. F. et al. Long-term culture, genetic manipulation and xenotransplantation of human normal and breast cancer organoids. *Nat. Protoc.* **16**, 1936–1965 (2021).
67. Picon-Ruiz, M., Marchal, J. A. & Slingerland, J. M. Obtaining human breast adipose cells for breast cancer cell co-culture studies. *STAR Protoc.* **1**, 100197 (2020).
68. Shalabi, S. F. et al. Evidence for accelerated aging in mammary epithelia of women carrying germline *BRCA1* or *BRCA2* mutations. *Nat. Aging* **1**, 838–849 (2021).
69. Gray, G. K. et al. A human breast atlas integrating single-cell proteomics and transcriptomics. *Dev. Cell* **57**, 1400–1420.e7 (2022).
70. Nyitray, C. E., Chavez, M. G. & Desai, T. A. Compliant 3D microenvironment improves β-cell cluster insulin expression through mechanosensing and β-catenin signaling. *Tissue Eng. Part A* **20**, 1888–1895 (2014).
71. Jeong, G. S. et al. Viscoelastic lithography for fabricating self-organizing soft micro-honeycomb structures with ultra-high aspect ratios. *Nat. Commun.* **7**, 11269 (2016).
72. Girgin, M. U. et al. Bioengineered embryoids mimic post-implantation development in vitro. *Nat. Commun.* **12**, 5140 (2021).
73. Wise, K. D. & Najafi, K. Microfabrication techniques for integrated sensors and Microsystems. *Science* **254**, 1335–1342 (1991).
74. Leong, T. G., Zarafshar, A. M. & Gracias, D. H. Three-dimensional fabrication at small size scales. *Small* **6**, 792–806 (2010).
75. Steedman, M. R., Tao, S. L., Klassen, H. & Desai, T. A. Enhanced differentiation of retinal progenitor cells using microfabricated topographical cues. *Biomed. Microdevices* **12**, 363–369 (2010).
76. Kharbikar, B. N., Kumar, S. H., Kr, S. & Srivastava, R. Hollow silicon microneedle array based trans-epidermal antiemetic patch for efficient management of chemotherapy induced nausea and vomiting. In *Micro + Nano Materials, Devices, and Systems Vol. 9668* (eds Eggleton, B. J. & Palomba, S.) 256–272 (SPIE, 2015).
77. Bernards, D. A. et al. Injectable devices for delivery of liquid or solid protein formulations. *ACS Materials Au* **3**, 255–264 (2023).
78. Kharbikar, B. N., Chendke, G. S. & Desai, T. A. Modulating the foreign body response of implants for diabetes treatment. *Adv. Drug Deliv. Rev.* **174**, 87–113 (2021).
79. Kharbikar, B. N., Mohindra, P. & Desai, T. A. Biomaterials to enhance stem cell transplantation. *Cell Stem Cell* **29**, 692–721 (2022).
80. Shukla, L., Yuan, Y., Shayan, R., Greening, D. W. & Karnezis, T. Fat therapeutics: the clinical capacity of adipose-derived stem cells and exosomes for human disease and tissue regeneration. *Front. Pharmacol.* **11**, 158 (2020).
81. White, J. D., Dewal, R. S. & Stanford, K. I. The beneficial effects of brown adipose tissue transplantation. *Mol. Aspects Med.* **68**, 74–81 (2019).
82. Liu, X. et al. Brown adipose tissue transplantation improves whole-body energy metabolism. *Cell Res.* **23**, 851–854 (2013).
83. Stanford, K. I. et al. Brown adipose tissue regulates glucose homeostasis and insulin sensitivity. *J. Clin. Invest.* **123**, 215–223 (2013).
84. Liu, X. et al. Brown adipose tissue transplantation reverses obesity in Ob/Ob mice. *Endocrinology* **156**, 2461–2469 (2015).
85. Pogodzinski, D., Ostrowska, L., Smakuls-Zarzecka, J. & Zysk, B. Secretome of adipose tissue as the key to understanding the endocrine function of adipose tissue. *Int. J. Mol. Sci.* **23**, 2309 (2022).
86. Sun, T. et al. Engineered adipose-derived stem cells overexpressing RXFP1 via CRISPR activation ameliorate erectile dysfunction in diabetic rats. *Antioxidants* **12**, 171 (2023).
87. Rudolph, M. C., Wellberg, E. A. & Anderson, S. M. Adipose-depleted mammary epithelial cells and organoids. *J. Mammary Gland Biol. Neoplasia* **14**, 381–386 (2009).
88. Currie, C. J., Poole, C. D. & Gale, E. A. The influence of glucose-lowering therapies on cancer risk in type 2 diabetes. *Diabetologia* **52**, 1766–1777 (2009).
89. Hemkens, L. G. et al. Risk of malignancies in patients with diabetes treated with human insulin or insulin analogues: a cohort study. *Diabetologia* **52**, 1732–1744 (2009).
90. Godsland, I. F. Insulin resistance and hyperinsulinaemia in the development and progression of cancer. *Clin. Sci. (Lond)* **118**, 315–332 (2009).
91. Nasiri, A. R., Rodrigues, M. R., Li, Z., Leitner, B. P. & Perry, R. J. SGLT2 inhibition slows tumor growth in mice by reversing hyperinsulinemia. *Cancer Metab.* **7**, 10 (2019).
92. Chondronikola, M. et al. Brown adipose tissue improves whole-body glucose homeostasis and insulin sensitivity in humans. *Diabetes* **63**, 4089–4099 (2014).
93. Chadt, A. & Al-Hasani, H. Glucose transporters in adipose tissue, liver, and skeletal muscle in metabolic health and disease. *Pflugers Arch.* **472**, 1273–1298 (2020).
94. Kousteni, S. FoxO1, the transcriptional chief of staff of energy metabolism. *Bone* **50**, 437–443 (2012).
95. Schilperoort, M. et al. The GPR120 agonist TUG-891 promotes metabolic health by stimulating mitochondrial respiration in brown fat. *EMBO Mol. Med.* **10**, e8047 (2018).
96. Satapati, S. et al. GPR120 suppresses adipose tissue lipolysis and synergizes with GPR40 in antidiabetic efficacy. *J. Lipid Res.* **58**, 1561–1578 (2017).
97. Nguyen, H. P. et al. Aifm2, a NADH oxidase, supports robust glycolysis and is required for cold- and diet-induced thermogenesis. *Mol. Cell* **77**, 600–617.e4 (2020).
98. Wang, P., Mariman, E., Renes, J. & Keijer, J. The secretory function of adipocytes in the physiology of white adipose tissue. *J. Cell. Physiol.* **216**, 3–13 (2008).
99. Bond, S. T., Calkin, A. C. & Drew, B. G. Adipose-derived extracellular vesicles: systemic messengers and metabolic regulators in health and disease. *Front. Physiol.* **13**, 837001 (2022).
100. Matharu, N. et al. CRISPR-mediated activation of a promoter or enhancer rescues obesity caused by haploinsufficiency. *Science* **363**, eaau0629 (2019).
101. Wang, X. et al. Evaluation and optimization of differentiation conditions for human primary brown adipocytes. *Sci. Rep.* **8**, 5304 (2018).
102. Lowell, B. B. & Flier, J. S. Brown adipose tissue, β3-adrenergic receptors, and obesity. *Annu. Rev. Med.* **48**, 307–316 (1997).
103. Sun, X. et al. Mirabegron displays anticancer effects by globally browning adipose tissues. *Nat. Commun.* **14**, 7610 (2023).

104. Chen, J., Guo, Z., Tian, H. & Chen, X. Production and clinical development of nanoparticles for gene delivery. *Mol. Ther. Methods Clin. Dev.* **3**, 16023 (2016).
105. Banskota, S. et al. Engineered virus-like particles for efficient in vivo delivery of therapeutic proteins. *Cell* **185**, 250–265.e16 (2022).
106. Tsagkaraki, E. et al. CRISPR-enhanced human adipocyte browning as cell therapy for metabolic disease. *Nat. Commun.* **12**, 6931 (2021).
107. Steele, C. B. et al. Vital signs: trends in incidence of cancers associated with overweight and obesity—United States, 2005–2014. *MMWR Morb. Mortal Wkly Rep.* **66**, 1052–1058 (2017).
108. Renehan, A. G., Zwahlen, M. & Egger, M. Adiposity and cancer risk: new mechanistic insights from epidemiology. *Nat. Rev. Cancer* **15**, 484–498 (2015).
109. Paz-Filho, G., Lim, E. L., Wong, M. L. & Licinio, J. Associations between adipokines and obesity-related cancer. *Front. Biosci. (Landmark Ed.)* **16**, 1634–1650 (2011).
110. Park, J., Morley, T. S., Kim, M., Clegg, D. J. & Scherer, P. E. Obesity and cancer—mechanisms underlying tumour progression and recurrence. *Nat. Rev. Endocrinol.* **10**, 455–465 (2014).
111. Sirin, O. & Kolonin, M. G. Treatment of obesity as a potential complementary approach to cancer therapy. *Drug Discov. Today* **18**, 567–573 (2013).
112. Khandekar, M. J., Cohen, P. & Spiegelman, B. M. Molecular mechanisms of cancer development in obesity. *Nat. Rev. Cancer* **11**, 886–895 (2011).
113. Huffman, D. M. et al. Cancer progression in the transgenic adenocarcinoma of mouse prostate mouse is related to energy balance, body mass, and body composition, but not food intake. *Cancer Res.* **67**, 417–424 (2007).
114. Zhang, Y. et al. Stromal progenitor cells from endogenous adipose tissue contribute to pericytes and adipocytes that populate the tumor microenvironment. *Cancer Res.* **72**, 5198–5208 (2012).
115. Wang, Y. Y. et al. Mammary adipocytes stimulate breast cancer invasion through metabolic remodeling of tumor cells. *JCI Insight* **2**, e87489 (2017).
116. Rohrig, F. & Schulze, A. The multifaceted roles of fatty acid synthesis in cancer. *Nat. Rev. Cancer* **16**, 732–749 (2016).
117. Beloribi-Djeafaflia, S., Vasseur, S. & Guillaumond, F. Lipid metabolic reprogramming in cancer cells. *Oncogenesis* **5**, e189 (2016).
118. Ye, H. et al. Leukemic stem cells evade chemotherapy by metabolic adaptation to an adipose tissue niche. *Cell Stem Cell* **19**, 23–37 (2016).
119. Cypess, A. M. Reassessing human adipose tissue. *N. Engl. J. Med.* **386**, 768–779 (2022).
120. Bashor, C. J., Hilton, I. B., Bandukwala, H., Smith, D. M. & Veiseh, O. Engineering the next generation of cell-based therapeutics. *Nat. Rev. Drug Discov.* **21**, 655–675 (2022).
121. Chendke, G. S. et al. Replenishable prevascularized cell encapsulation devices increase graft survival and function in the subcutaneous space. *Bioeng. Transl. Med.* **8**, e10520 (2023).
122. Kharbikar, B. N., Zhong, J. X., Cuylear, D. L., Perez, C. A. & Desai, T. A. Therapeutic biomaterials for tissue engineering. *Curr. Opin. Biomed. Eng.* **19**, 100299 (2021).
123. Herberts, C. A., Kwa, M. S. & Hermans, H. P. Risk factors in the development of stem cell therapy. *J. Transl. Med.* **9**, 29 (2011).
124. Buitinga, M. et al. Micro-fabricated scaffolds lead to efficient remission of diabetes in mice. *Biomaterials* **135**, 10–22 (2017).
125. Carpenter, R. et al. Scaffold-assisted ectopic transplantation of internal organs and patient-derived tumors. *ACS Biomater. Sci. Eng.* **5**, 6667–6678 (2019).
126. Cordeiro, P. G. Breast reconstruction after surgery for breast cancer. *N. Engl. J. Med.* **359**, 1590–1601 (2008).
127. Juntunen, M. et al. Evaluation of the effect of donor weight on adipose stromal/stem cell characteristics by using weight-discordant monozygotic twin pairs. *Stem Cell Res. Ther.* **12**, 516 (2021).
128. Chu, D. T. et al. Adipose tissue stem cells for therapy: an update on the progress of isolation, culture, storage, and clinical application. *J. Clin. Med.* **8**, 917 (2019).

Publisher's note Springer Nature remains neutral with regard to jurisdictional claims in published maps and institutional affiliations.

Open Access This article is licensed under a Creative Commons Attribution 4.0 International License, which permits use, sharing, adaptation, distribution and reproduction in any medium or format, as long as you give appropriate credit to the original author(s) and the source, provide a link to the Creative Commons licence, and indicate if changes were made. The images or other third party material in this article are included in the article's Creative Commons licence, unless indicated otherwise in a credit line to the material. If material is not included in the article's Creative Commons licence and your intended use is not permitted by statutory regulation or exceeds the permitted use, you will need to obtain permission directly from the copyright holder. To view a copy of this licence, visit <http://creativecommons.org/licenses/by/4.0/>.

© The Author(s) 2025

¹Department of Bioengineering and Therapeutic Sciences, University of California San Francisco, San Francisco, CA, USA. ²Institute for Human Genetics, University of California San Francisco, San Francisco, CA, USA. ³Department of Nutritional Sciences, University of Texas at Austin, Austin, TX, USA.

⁴Division of Hematology/Oncology, Department of Medicine, University of California San Francisco, San Francisco, CA, USA. ⁵Department of Medical Oncology, Dana-Farber Cancer Institute, Boston, MA, USA. ⁶Harvard Medical School, Boston, MA, USA. ⁷Department of Pathology, Brigham and Women's Hospital, Boston, MA, USA. ⁸Department of Laboratory Medicine, University of California San Francisco, San Francisco, CA, USA. ⁹Department of Pharmaceutical Chemistry, University of California San Francisco, San Francisco, CA, USA. ¹⁰University of California Davis West Coast Metabolomics Center, Davis, CA, USA. ¹¹Department of Surgery, University of California San Francisco, San Francisco, CA, USA. ¹²School of Engineering, Brown University, Providence, RI, USA. ¹³Chan Zuckerberg Biohub, San Francisco, CA, USA. ¹⁴Deceased: Hai P. Nguyen  e-mail: nadav.ahituv@ucsf.edu

Methods

Human and mouse adipocytes

For adipocyte differentiation, human preadipocytes or mouse 3T3-L1 preadipocytes were used (both kind gifts from H. Sook Sul, UC Berkeley). For human cells, the cell line was immortalized and a single-cell clone was established from primary preadipocytes (Cell Applications, 802S-05A). Cells were cultured to 100% confluence in DMEM, supplemented with 10% FBS, and fresh media was replaced. After 48 h, cells were subjected to adipocyte differentiation by adding a cocktail of IBMX (0.5 M) (Sigma-Aldrich, 410957), dexamethasone (1 μM) (Sigma-Aldrich, D1756) and insulin (10 μg ml⁻¹) (Sigma-Aldrich, I9278). The media was replaced every 2 days with insulin-containing DMEM complete media (Fisher Scientific, 11-965-118) during differentiation.

Cancer cell lines

All cancer cells were acquired from American Type Culture Collection (ATCC). MCF-7 cells (ATCC, HTB-22) were cultured in Eagle's minimum essential medium (ATCC, 30-2003), supplemented with 10% FBS and 10 μg ml⁻¹ human recombinant insulin (Sigma-Aldrich, I9278). MDA-MB-436 cells (ATCC, HTB-130) were cultured in Leibovitz's L-15 medium (ATCC, 30-2008) with 10 μg ml⁻¹ insulin, 16 μg ml⁻¹ glutathione (Sigma-Aldrich, G6013) and 10% FBS. SW-1417 cells (ATCC, CCL-238) were grown in Leibovitz's L-15 medium supplemented with 10% FBS. PANC10.05 cells (ATCC, CRL-2547) were cultured in RPMI-1640 medium (ATCC, 30-2001) with 10 μg ml⁻¹ human insulin and 15% FBS. DU-145 cells (ATCC, HTB-81) were cultured in Eagle's minimum essential medium with 10% FBS. PANC-1 cells (ATCC, CRL-1469) were cultured in DMEM medium (ATCC, 30-2002) supplemented with 10% FBS.

CRISPRa-AAV in vitro optimization

Five gRNAs targeting the promoter of human *UCP1*, *PPARGC1A*, *PRDM16* and *UPP1* or mouse *Ucp1* were designed using CRISPICK¹²⁹ (Supplementary Table 3). These guides were individually cloned into pAAV-U6-sasgRNA-CMV-mCherry-WPREpA¹⁰⁰ (Addgene, 217015) at the BstXI and Xhol restriction enzyme sites using the In-Fusion (Takara Bio, 638910) cloning method¹⁰⁰. A total of 5×10^5 human preadipocytes or mouse 3T3-L1 cells were plated onto 12-well plates and then subjected to the adipocyte differentiation protocol after 2 days of confluence. At day 4 of differentiation, cells were transfected with 0.5 μg of dCas9-VP64 and 0.5 μg of gRNA plasmid using X-tremeGene (Sigma-Aldrich, 6366236001) and CombiMag reagent (OZ Biosciences, CM21000) following the manufacturer's protocol. At day 8 of differentiation, cells were lysed with Trizol, RNA was collected and cDNA and RT-qPCR were performed as described in the 'RNA isolation and RT-qPCR' section below. The two gRNAs with the highest upregulation for each gene were packaged into rAAV9 serotype virions. rAAV9 serotype virions were produced by transfecting AAVpro 293T cells (Takara, 632273) with pCMV-sadCas9-VP64 (Addgene, 115790) or pAAV-U6-sasgRNA-CMV-mCherry-WPREpA¹⁰⁰ along with packaging vectors, including PAAV2/9n (Addgene, 112865) and pHelper vectors using TransIT293 reagent (Mirus, 2700). After 72 h, AAV particles were collected and purified using the AAVpro Cell & Sup. Purification Kit Maxi (Takara, 6676) and quantified by the AAVpro Titration Kit (Takara, 6233). gRNA AAV (1×10^6 multiplicity of infection (MOI)) and dCas9-VP64 AAV (1×10^6 MOI) were used to infect human and mouse differentiated adipocytes. After 5 days, RNA was collected, cDNA was prepared and RT-qPCR was carried out as described below.

RNA isolation and RT-qPCR

Total RNA from sorted or cultured cells was extracted using Trizol reagent (Thermo Fisher, 15596026). Reverse transcription was performed with 1 μg of total RNA using the qScript cDNA Synthesis Kit (Quantabio, 95047) following the manufacturer's protocol. RT-qPCR was performed on the QuantStudio 6 Real-Time PCR System (Thermo Fisher) using Sso Fast (Bio-Rad, 1725205). Statistical analysis was

performed using ΔΔCt method with *Gapdh* primers as a control (see primer sequences in Supplementary Table 3).

Seahorse assay

Human preadipocytes (5×10^5 cells per well) were plated in 12-well plates and subjected to the adipocyte differentiation protocol. Adipocytes and cancer cell lines were trypsinized and reseeded in XF96 plates (Agilent, 102905-100) at 2×10^4 cells per well and assayed the next day. On the day of the experiments, the cells were washed two times and maintained in XF base medium (Agilent, 103334) supplemented with either 1 mM sodium pyruvate (Thermo Fisher, 11360070) and 17.5 mM glucose (Sigma-Aldrich, G7021) for the mitochondria stress test or 2 mM glutamine (StemCell technologies, 07100) for the glycolysis test. For FAO tests, cells were washed and incubated with substrate-limiting medium DMEM (Corning, 17-207-CV) supplemented with 0.5 mM glucose, 1 mM GlutaMAX (Thermo Fisher, 35050061), 0.5 mM carnitine (Sigma-Aldrich, C0283) and 1% FBS. Cells were incubated at 37 °C in a non-CO₂ incubator for 1 h. The assay was performed using a Seahorse XFe96 analyzer (Agilent, XFe96). Oxygen consumption was measured under 1.5 μM oligomycin (Sigma-Aldrich, 75351), 2 μM FCCP (Sigma-Aldrich, C2920) and 0.5 μM Rotenone (Sigma-Aldrich, R8875) and antimycin (Sigma-Aldrich, A8674). The ECAR was measured under 10 mM glucose, 1 μM oligomycin and 50 mM 2-deoxyglucose (Sigma-Aldrich, D8375).

Glucose uptake assay

Human preadipocytes (3×10^5 cells per well) were plated in 96-well tissue culture plates and subjected to the adipocyte differentiation protocol. The day before the assay, the media was replaced with low serum-free media. On the day of the assay, using glucose uptake-Glo assay (Promega, J1342), cells were incubated with 1 nM insulin (Sigma-Aldrich, I9278) for 1 h before the assay following the manufacturer's protocol.

Fatty acid uptake assay

Human preadipocytes (3×10^5 cells per well) were plated in 96-well tissue culture plates and subjected to the adipocyte differentiation protocol or 1×10^5 human mammary gland adipocytes were plated in 96-well plates. On the day of the assay, the media was replaced with serum-free media. Using the fatty acid uptake kit (Sigma-Aldrich, MAK156), cells were incubated with 1 nM insulin (Sigma-Aldrich, I9278) for 30 min before the assay following the manufacturer's protocol.

Western blot

To generate a UCP1-positive control, 2 μg of a FLAG-tagged human UCP1 plasmid (Origene, RC218901) was mixed with 200 μl of Opti-MEM (Fisher Scientific, 31985062) and 4 μl of X-tremeGENE HP DNA Transfection Reagent (Roche, XTGHP-RO) and incubated for 15 min. The mixture was added onto AAVpro 293T cells (Takara, 632273) at 6×10^5 per well in a six-well plate and cells were collected 48 h after the transfection. Cells for all conditions were washed twice with DPBS (Sigma-Aldrich, D8537) and dissolved with RIPA buffer (Fisher Scientific, P189900) containing proteinase inhibitor cocktails and EDTA (Fisher Scientific, P178440). After shaking for 5 min at 4 °C, cell lysates were centrifuged at 12,000g at 4 °C for 10 min to collect the supernatant, and protein concentrations were determined with a BCA protein assay kit (Fisher Scientific, 23227). The cell lysate was mixed with Laemmli SDS sample buffer, reducing (6X) (Fisher Scientific, J61337.AD) to prepare a 1 μg μl⁻¹ concentration and placed at 95 °C for 5 min in a programmed heat block. SDS-PAGE was performed on the denatured lysate (10 μg per lane for GAPDH and 40 μg ml⁻¹ for other conditions) using Bolt Bis-Tris Mini Protein Gels, 4–12%, 1.0 mm (Fisher Scientific, NW04120BOX) and Bolt MES SDS Running Buffer (Fisher Scientific, B0002). PageRuler Plus Prestained Protein Ladder (Fisher Scientific, 26619) was used as a molecular weight marker. The gels were transferred onto membranes using iBlot2 (Fisher Scientific, IB23002). The membranes were blocked with PVDF Blocking

Reagent for Can Get Signal (Toyobo, NYPBR01) for 1 h and treated with primary antibody solutions for hGAPDH and hUCP1 (antibody information in Supplementary Table 4) diluted 1,000-fold with Can Get Signal solution 1 (Toyobo, NKB-101) overnight at 4 °C. The membranes were washed twice with DPBS containing 0.02% Tween 20 (Bio-Rad, 1706531) and a secondary antibody solution diluted with Can Get Signal solution 2 was added (Toyobo, NKB-101). After incubation for 1 h at 20 °C room temperature, the membranes were washed twice with DPBS containing 0.02% Tween 20. Antigens were detected with the ECL 2 Western Blotting Substrate detection reagent (Fisher Scientific, PI80196) and imaged on an ImageQuant 800 (Cytiva).

Co-culturing CRISPRa-modulated adipocytes with cancer cells

A total of 5×10^5 human preadipocytes were plated in 12-well tissue culture plates and subjected to the adipocyte differentiation protocol. On day 2 of differentiation, cells were transduced with gRNA AAV (1×10^6 MOI) and dCas9–VP64 AAV (1×10^6 MOI). After 6 days, cells were collected and replated into the upper well of a 12-well Transwell plate (Corning, 07-200-150) in which 3×10^5 cancer cells had been plated in the lower well 1 day earlier. The cells were cultured in the adipocyte differentiation media (as described previously) and designated media for each cancer cell line (1:1 ratio). For PANC-1, cells were incubated with or without the addition of 1 mM uridine. After 3 days, cancer cells were collected for imaging, cell viability assay or seahorse assay. RNA was collected, cDNA was prepared and RT-qPCR was carried out as previously described. Differential expression was determined using the ΔΔCt method with GAPDH primers as control (primer sequences in Supplementary Table 3).

Luminescent cell viability

MCF-7 cells were grown as mentioned above and treated for 3 days with either CRISPRa-UCP1-AAV adipocytes or dCas9–VP64 as a negative control; 6-aminonicotinamide (Sigma-Aldrich, A68203) at 50 μM or 100 μM with DMSO as negative control; and etomoxir (Sigma-Aldrich, E1905) at 100 μM or 200 μM with DMSO as a negative control. The luminescent cell viability assay was performed using the CellTiter-Glo Luminescent Cell Viability Assay (Promega, G7570) following the manufacturer's protocol on four biological replicates per condition.

Human and mouse adipose organoid culture

Human or mouse 3T3-L1 preadipocytes (0.5×10^6 cells) were plated in 96-well Nunclon Sphera ULA U-bottom plates (Thermo Fisher, 174929). Organoids formed after 48 h and were then differentiated into adipose organoids using a differentiation cocktail containing IBMX (0.5 M), dexamethasone (1 μM) and insulin (10 μg ml⁻¹). Adipocytes formed 21 days post differentiation. Human adipose organoids were then transduced with gRNA AAV (1×10^6 MOI) and dCas9–VP64 AAV (1×10^6 MOI). After 5 days, organoids were collected and mixed with Matrigel (Corning, 354234) and subcutaneously injected into mice (ten organoids per mouse).

Co-transplantation of CRISPRa-modulated human adipose organoids and cancer cells

All animal studies were carried out in accordance with the University of California San Francisco (UCSF) Institutional Animal Care and Use Committee, protocol number AN197608. Mice were housed in a 12 h:12 h light-to-dark cycle; chow diet (Envigo, 2018S) and water were provided ad libitum. Immune-deficient SCID mice (5 weeks old; JAX, 001303) were anesthetized using isoflurane and subcutaneously injected with 2×10^6 – 6×10^6 cancer cells, or $\sim 2 \times 10^6$ cells after trypsinization of tumor organoids and mixed 1:1 with Matrigel, in PBS. After 6–12 weeks, depending on the cancer cell lines, the mice were subcutaneously injected with CRISPRa-AAV human adipocytes or adipose organoids to a site adjacent to the tumor. After 3–6 weeks, mice were killed and tumors and adipose implants were collected. Tumor size was

measured with calipers and tumor volume was determined according to the standard formula (length × width² × 0.52).

Immunofluorescence

A portion of the isolated tumors was fixed with 1% paraformaldehyde for 2 h and prepared for cryostat sectioning. Each sample was cut into 5 μm-thick sections and blocked with 3% BSA (Miltenyi Biotec, 130-091-376) blocking solution for 30 min. For Ki67 staining, slides were permeabilized with 1% Triton X-100 PBS solution for 15 min and washed with 0.1% Tween 20 PBS solution before blocking. Slides were then incubated with primary antibodies (information and concentrations are listed in Supplementary Table 4) overnight at 4 °C and washed three times with 0.1% Tween 20 PBS. The slides were then incubated with secondary antibodies (information and concentrations are listed in Supplementary Table 4) for 60 min at room temperature and then washed three times with 0.1% Tween 20 PBS. Images were obtained using a confocal microscope (Zeiss, LSM880) and analyzed with Fiji¹³⁰.

Whole-mount staining

Adipose organoids collected after implantation were fixed with 2% paraformaldehyde overnight and then stained with LipidTox Red (Thermo Fisher, H34476) (1:1,000) for 2 h. Images were acquired using a confocal microscope (Zeiss, LSM880).

Metabolic and thermogenic measurements

Oxymax–CLAMS (Columbus Instruments) was used to measure oxygen consumption and carbon dioxide production of individual mice. Mice were housed individually at 30 °C, 16 °C and 4 °C under a 12 h:12 h light-to-dark cycle. Food and water were available ad libitum. We calculated the respiratory exchange ratio by dividing the volume of CO₂ produced by the volume of O₂ consumed.

RNA-seq analysis

Total RNA was isolated from tumors using the RNeasy Plus kit (Qiagen, 74136). Sequencing libraries were prepared using TruSeq Stranded Total RNA Library Prep Kit (Illumina) and sequenced by Novogene using Illumina NovaSeq 6000. Using Partek Flow (Illumina), reads were trimmed and aligned to the human genome (hg38) using STAR¹³¹. Differentially expressed genes were annotated using Limma-voom¹³² and were defined as those that were induced at least \pm fourfold, and their expression was significantly different from the basal (5% false discovery rate-adjusted $P < 0.01$). We used Geneontology.org (<https://geneontology.org/>)^{62,63} to determine gene ontology enrichment using biological processes annotations with Fisher's Exact test and a 5% false discovery rate-adjusted P value of <0.0001 . RNA-seq data are available under GEO accession number GSE246231 (ref. 133).

CRISPRa-modulated mouse adipose organoid implantation in genetic mouse models

KPC, a tamoxifen-inducible *Kras*^{LSL-G12D}; *p53*^{LOXP}; *Pdx1-creER* triple-mutant model of tamoxifen-inducible PDA on a C57/BL6 background, was acquired from the Jackson Laboratory (strain no. 032429). To induce Cre recombination, tamoxifen was administered to pups through lactation following oral gavage of the mother with 6 mg tamoxifen (suspended in corn oil) on postnatal days 0, 1, 2 and 4. We orthotopically implanted mouse adipose organoids (ten organoids per mouse) mixed with Matrigel (Corning, 354234) near the pancreas in 4-week-old mice, using a method similar to a previously published protocol¹³⁴, and dissected the pancreas 6 weeks after the implantation. The *MMTV-PyMT* breast cancer mice were acquired from the Jackson Laboratory (strain no. 002374). Female mice were implanted with mouse adipose organoids at 4 weeks of age (ten organoids per mouse) mixed with Matrigel (Corning, 354234) and subcutaneously injected into mice either at the third nipple or on the back. The tumors were collected 6 weeks post implantation.

Cancer organoids

Organoids were generated from breast tumor tissue or tumors from malignant effusions. Patients provided their consent for specimen collection using IRB-approved tissue collection protocols at the UCSF and the Brigham and Women's Hospital. Surgical specimens were obtained from the UCSF Medical Center or Brigham and Women's Hospital on the day of their procedure, viably frozen as tissue pieces or used to generate formalin-fixed, paraffin-embedded sections or organoid cultures. Each tissue was minced using razor blades and digested in a solution containing DMEM/F12 (Gibco, 11330), 2 mM GlutaMAX (Gibco, 35050), 10 mM HEPES (Gibco, 15630), 50 U ml⁻¹ penicillin-streptomycin (Gibco, 15070) and 1 mg ml⁻¹ collagenase XI (Sigma-Aldrich, C9407). Tissue digestion was performed at 37 °C with constant shaking at 150 rpm for 1–2 h. Cells were then pelleted by centrifugation, further dissociated by sequentially pipetting with 10 ml, 5 ml and 1 ml pipette tips and then re-centrifuged. The resulting cell pellet was used directly to establish organoid cultures by embedding in basement membrane extract, allowing this to harden at 37 °C for 20 min to form a hydrogel dome and then overlaying this dome with Type 1 Organoid Medium as previously described^{69,135}. All metastatic cancer organoids were derived from malignant pleural effusions that were collected from patients with metastatic breast cancer who were undergoing thoracentesis at the UCSF Medical Center. The fluid samples were placed on ice within 4 h after collection. Organoids were generated by washing malignant effusions with PBS, collecting tumor spheroids by centrifugation and incubating with 3–5 ml RBC lysis buffer (BioLegend, 420301) for 10–15 min when there were visible RBCs, followed by embedding the cell pellet in organoid culture as described above.

Metabolomics

The tumors were collected and subjected to metabolomics analysis to measure primary metabolites by the University of California Davis West Coast Metabolomics Center. The data were normalized to tumor mass (Supplementary Table 1).

Mammary gland adipocyte isolation

For adipocyte extraction, mammary gland adipose tissues from excess tissue removed during breast surgeries were washed with PBS three times and mechanically minced into smaller pieces. The tissue mixture was incubated with PBS with 3% BSA and collagenase I (1 mg ml⁻¹) for 45 min at 37 °C and then centrifuged; the top lipid layer was then discarded. The remaining mixture was filtered twice through a 200 µm strainer and centrifuged. Mature adipocytes were isolated and washed twice with PBS and then plated in suspension in six-well plates in high-glucose DMEM media supplemented with 10% FBS. For transduction of CRISPRa, *UCP1* AAV9 (1×10^6 MOI) and dCas9–VP64 AAV9 (1×10^6 MOI) were mixed with 20 µl of AdeoMag (OZ Biosciences, AM71000) and adipocytes and incubated for 15 min. The virus and cell mixture was distributed onto a six-well plate placed upon the magnetic plate and incubated for 15 more minutes.

Co-culturing of cancer organoids and adipocytes

At 5 days post infection of CRISPRa AAV9, adipocytes were placed in a tissue Transwell culture plate (Corning, 07-200-150) of tumor organoids at a 1:1 ratio of adipocyte media and breast cancer organoid media. Cells were incubated for up to 7 days and then examined for adipocyte and tumor phenotypes.

Co-implantation of cancer organoids and adipocytes

Immune-deficient SCID mice (5 weeks old; JAX, 001303) were anesthetized using isoflurane and subcutaneously injected with 3×10^5 cancer organoids mixed 1:1 with Matrigel in PBS. After 3 weeks, we subcutaneously injected CRISPRa-AAV mammary adipocytes mixed with Matrigel to a site adjacent to the tumor. After another 3 weeks, tumors and adipose implants were dissected. We measured tumor size

with calipers and determined tumor volume according to the standard formula (length × width² × 0.52).

Tet-On CRISPRa

The rtTA was amplified from pSBtet-GP (Addgene, 60495) along with a sequence encoding for T2A and cloned downstream of the *CMV* promoter in the gRNA-AAV vector digested with NheI and AgeI. The TRE and a minimal promoter were amplified and cloned upstream of dCas9–VP64 in the dCas9–VP64 AAV vector digested with XbaI and AgeI. After adipose organoids were infected with Tet-On *UCP1*-CRISPRa and implanted, mice were fed with a doxycycline diet (Bio-Serv, S3888).

PCL microwell scaffold fabrication

Microwell scaffolds were fabricated using a combination of micro-fabrication techniques, including photolithography and micromolding. We used PCL (Sigma-Aldrich, 440744), a biocompatible polymer to fabricate microwell scaffolds. We used a polymer blend of 150 mg ml⁻¹ PCL (molecular weight, 80K; Sigma-Aldrich, 9016-00-6) and polyethylene glycol (molecular weight, 2.5K; Sigma-Aldrich, 438197) in trifluoroethanol (Sigma-Aldrich, 8.08259). The polymer solution was stirred on the roller bank overnight at room temperature. We then used photolithography to fabricate the SU8 (Microchem/Kayaku, Y111075) microwell array master mold. The microwell mold was then silanized and polydimethylsiloxane (PDMS) (Thermo Fisher, 178442500) and was used to prepare the microwell template. The PDMS template had a micropatterned spatially organized array of dome-like structures called microwells, each 700 µm in height and 500 µm diameter. Micromolding was used to prepare the PCL microwell scaffold using a PDMS microwell template. Two-step spin casting was used to cast the PCL solution on the PDMS microwell template at 100 rpm and 1,000 rpm for 10 s to regulate the height of the microwell; the microwell diameter was defined by the microwells on the template. The PCL-coated template was allowed to dry at room temperature overnight to evaporate the organic solvent, followed by immersion in deionized water. The polyethylene glycol in the PCL polymer blend was allowed to leach out in a deionized water bath for 5 days to introduce the porosity in the microwell PCL scaffold. Subsequently, the microwell scaffolds were washed and stored in deionized water till further use. The size of the microwells on the PCL micro-well scaffold was designed to be suitable to host adipose organoids.

Adipose organoids microwell scaffold transplantation

The microwell scaffold organoid delivery platform was primed for the transplantation of adipose organoids. The microwell scaffolds were thoroughly washed and dried followed by treatment with air plasma for 3 min in aseptic conditions. We then soaked the scaffolds in a solution of adipocyte differentiation media and Matrigel (Corning, 354234) at 4 °C for 24 h. The adipose organoids were then spin-loaded individually in each microwell at 1,000 rpm and 4 °C. The microwell scaffolds loaded with adipose organoids were then layered with a 1:1 ratio of adipocyte differentiation media and Matrigel. The scaffold-organoids system was then cultured at 37 °C at 5% CO₂ for 24 h. The immunodeficient SCID mice (JAX, 001303) were antecently prepped with orthotopic MCF-7 tumor. The adipose organoids-loaded microwell organoid delivery scaffolds were then transplanted into the mice adjacent to the orthotopic tumor. After 3 weeks, tumors and microwell scaffold adipose organoid implants were collected. The tumor size was measured with calipers and tumor volume was determined according to the standard formula (length × width² × 0.52).

Scanning electron microscopy

Adipose organoids on the microwell scaffolds were meticulously prepared for analysis and visualization of their ultrastructural characteristics using SEM. The organoids on the scaffolds were fixed by immersing them in a 2.5% glutaraldehyde (Electron Microscopic Sciences, 16210) solution in a 0.1 M sodium cacodylate (Sigma-Aldrich, C0250) buffer with a pH of

7.2 at 4 °C over 24 h. Subsequently, samples were thoroughly rinsed for 30 min with 0.1 M sodium cacodylate buffer with a pH of 7.4 to remove residual fixative. To enhance structural contrast, post-fixation was performed using a 2% phosphotungstic acid (Sigma-Aldrich, P4006) in 0.1 M sodium cacodylate buffer at 4 °C for 1 h followed by thoroughly rinsing for 30 min with 0.1 M sodium cacodylate buffer with a pH of 7.4. The samples were then dehydrated by immersing for 20 min each in a graded series of ethanol (35%, 50%, 70%, 95%, 100%) solutions, enabling the gradual removal of water content. Critical-point drying over 24 h using hexamethyldisilazane (Sigma-Aldrich, 440191) ensured the complete removal of moisture from the specimens without causing any damage. Finally, a thin iridium coating of ~2 nm thickness was sputter-coated on the samples to enhance conductivity during SEM imaging. This systematic sample preparation method facilitated high-resolution SEM imaging at 1 kV on Phenom Pharos G2 Desktop FEG-SEM (Thermo Fisher Scientific), enabling a comprehensive exploration of the ultrastructural morphology.

Uridine and uridine triphosphate (UTP) uptake studies

Adipocytes differentiated and treated with or without *UPP1*-CRISPRa were maintained in a 24-well plate using cell culture medium (see ‘Cell culture media’ section). Before the uptake experiments, the culture medium was discarded and the cells were incubated in 1.0 ml of Hanks’ balanced salt solution (HBSS; Gibco, 14025092) for 10–20 min at 37 °C. After this pre-incubation, trace amounts of either ³H-uridine (128 nM) or 3H-UTP (240 nM) were introduced to the cells and incubation continued for 1 h or 12 h. Subsequently, the cells were washed twice with ice-cold HBSS. After washing, the cells were lysed using a lysis buffer composed of 0.1 N NaOH and 0.1% SDS. The radioactivity in the lysate was then quantified through liquid scintillation counting.

Statistical analysis

Statistical analyses were performed using one-way ANOVA or two-tailed *t*-tests and are described in each figure legend. A *P* value of <0.05 was considered statistically significant. The number of mice or replicates used in each experiment are indicated in the figure legends.

Reporting summary

Further information on research design is available in the Nature Portfolio Reporting Summary linked to this article.

Data availability

All data are available upon request. Requests for materials should be directed to the corresponding author. RNA-seq data are available under GEO accession number [GSE246231](#) (ref. 133). Source data are provided with this paper.

References

129. Doench, J. G. et al. Optimized sgRNA design to maximize activity and minimize off-target effects of CRISPR–Cas9. *Nat. Biotechnol.* **34**, 184–191 (2016).
130. Schindelin, J. et al. Fiji: an open-source platform for biological-image analysis. *Nat. Methods* **9**, 676–682 (2012).
131. Dobin, A. et al. STAR: ultrafast universal RNA-seq aligner. *Bioinformatics* **29**, 15–21 (2013).
132. Law, C. W., Chen, Y., Shi, W. & Smyth, G. K. voom: precision weights unlock linear model analysis tools for RNA-seq read counts. *Genome Biol.* **15**, R29 (2014).
133. H. P. Nguyen, et al. Project ID GSE246231. *Gene Expression Omnibus* <https://www.ncbi.nlm.nih.gov/geo/query/acc.cgi?acc=GSE246231> (2024).
134. Qiu, W. & Su, G. H. Development of orthotopic pancreatic tumor mouse models. *Methods Mol. Biol.* **980**, 215–223 (2013).
135. Rosenbluth, J. M. et al. Organoid cultures from normal and cancer-prone human breast tissues preserve complex epithelial lineages. *Nat. Commun.* **11**, 1711 (2020).

Acknowledgements

This paper is dedicated to Dr. Hai P. Nguyen, an outstanding scientist, colleague and friend who left this world prematurely. We thank the Shkedy sisters (Nurit Ahituv, Liora Parzelina), Felix Feng and Rachel Chan, Ethan Freed, Cameron Pitzak and the Las Lomas High School cancer club for inspiring this study. We thank Hei Sook Sul for her support and kindly providing the human preadipocyte cell line, the UC Davis West Coast Metabolomics Center for metabolomic assays and the patients who provided clinical material. We would also like to thank Coline Arnould, Felix Feng and Alan Ashworth from UCSF for their support and advice. This work was funded in part by the UCSF Sandler Program for Breakthrough Biomedical Research, which is partially funded by the Sandler Foundation (to J.M.R. and N.A.), Susan G. Komen Foundation (J.M.R.), METAvivor (J.M.R.), DF/HCC Breast SPORE: Specialized Program of Research Excellence (SPORE), a National Cancer Institute (NCI) funded program, Grant 1P50CA168504, UCSF Benioff Initiative for Prostate Cancer Research (N.A.), National Institute of Diabetes and Digestive and Kidney Disease 1R01DK124769 (N.A.), the UCSF Living Therapeutics Initiative (N.A.), NCI grant number 1R01CA283826 (J.M.R., N.A.), University of California Office of the President (UCOP) California Breast Cancer Research Program (CBCRP) IDEA grant (M.J.M.M.) and NCI grant number R01CA292019 (M.J.M.M., J.M.R.), and the California Institute for Regenerative Medicine (CIRM) postdoctoral fellowship (H.P.N., S.L.F.), CIRM Bridges Science Master’s Fellowship (SFU EDUC2-12693) (B.P.) and the National Human Genome Research Institute 1K99HG012576 (A.U.). The content is solely the responsibility of the authors and does not necessarily represent the official views of the National Institutes of Health.

Author contributions

H.P.N. and N.A. conceived the study. H.P.N., K.A., Y.I., R.S., M.B., B.P., K.P., H.H., E.M., X.Z., C.B., A.U., J.A.K. and S.W.Y. devised the methodology. J.M.R., F.L., D.A.D., M.J.M.M., L.A.H. and L.E. collected and worked with the human samples. B.N.K., D.A.B. and T.A.D. generated and worked on the integrated cell-scaffold delivery platform device. L.V. and O.F. performed the metabolomics analysis. H.P.N., M.N., S.L.F. and N.A. visualized the study. N.A. supervised the project. N.A. and J.M.R. acquired funding. H.P.N. and N.A. wrote, reviewed and edited the paper with contributions from all authors.

Competing interests

N.A. is a cofounder and on the scientific advisory board of Regel Therapeutics. N.A. receives funding from BioMarin Pharmaceutical Incorporate. H.P.N. and N.A. have filed a patent application covering embodiments and concepts disclosed in the paper. The other authors declare no competing interests.

Additional information

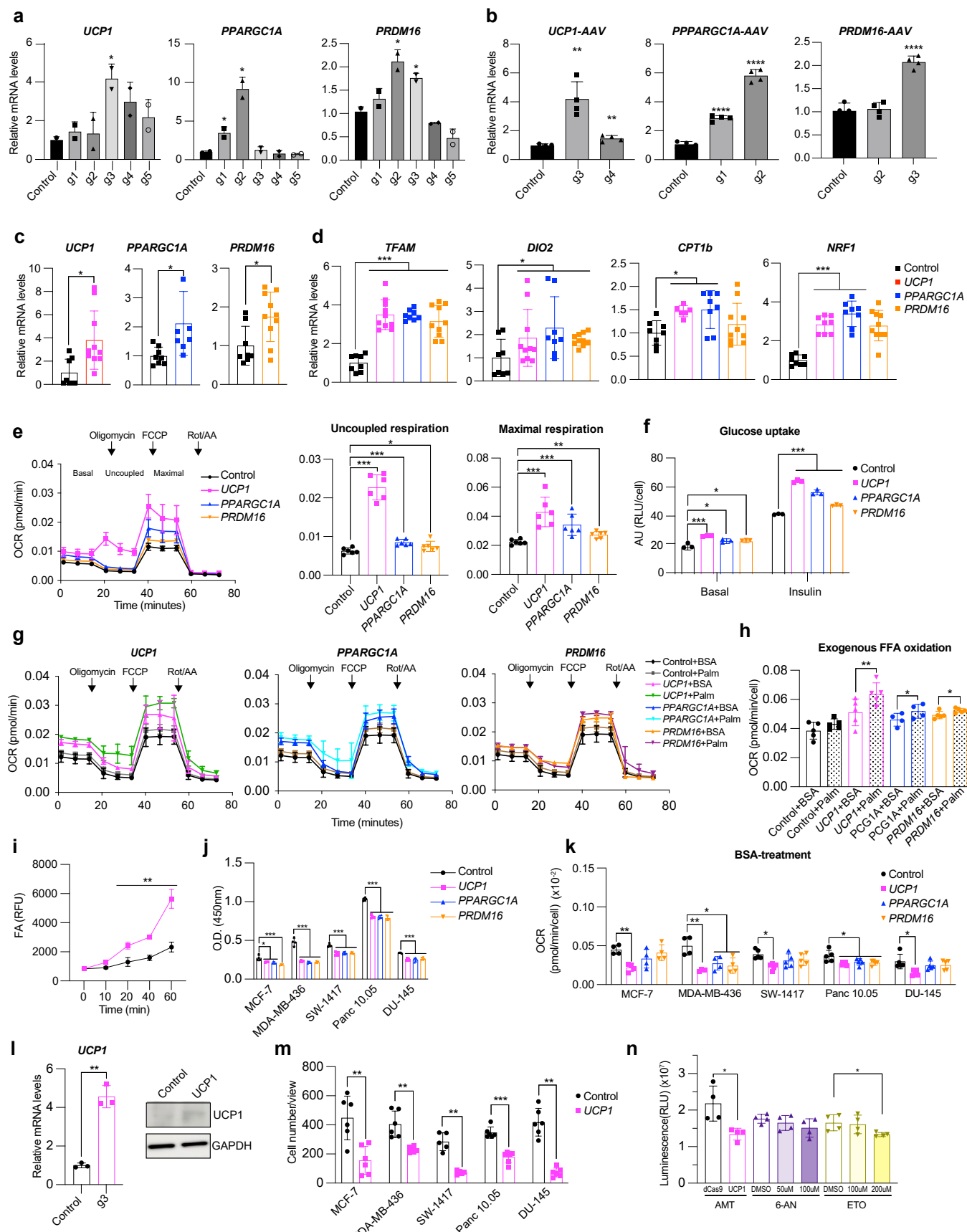
Extended data is available for this paper at <https://doi.org/10.1038/s41587-024-02551-2>.

Supplementary information The online version contains supplementary material available at <https://doi.org/10.1038/s41587-024-02551-2>.

Correspondence and requests for materials should be addressed to Nadav Ahituv.

Peer review information *Nature Biotechnology* thanks the anonymous reviewers for their contribution to the peer review of this work

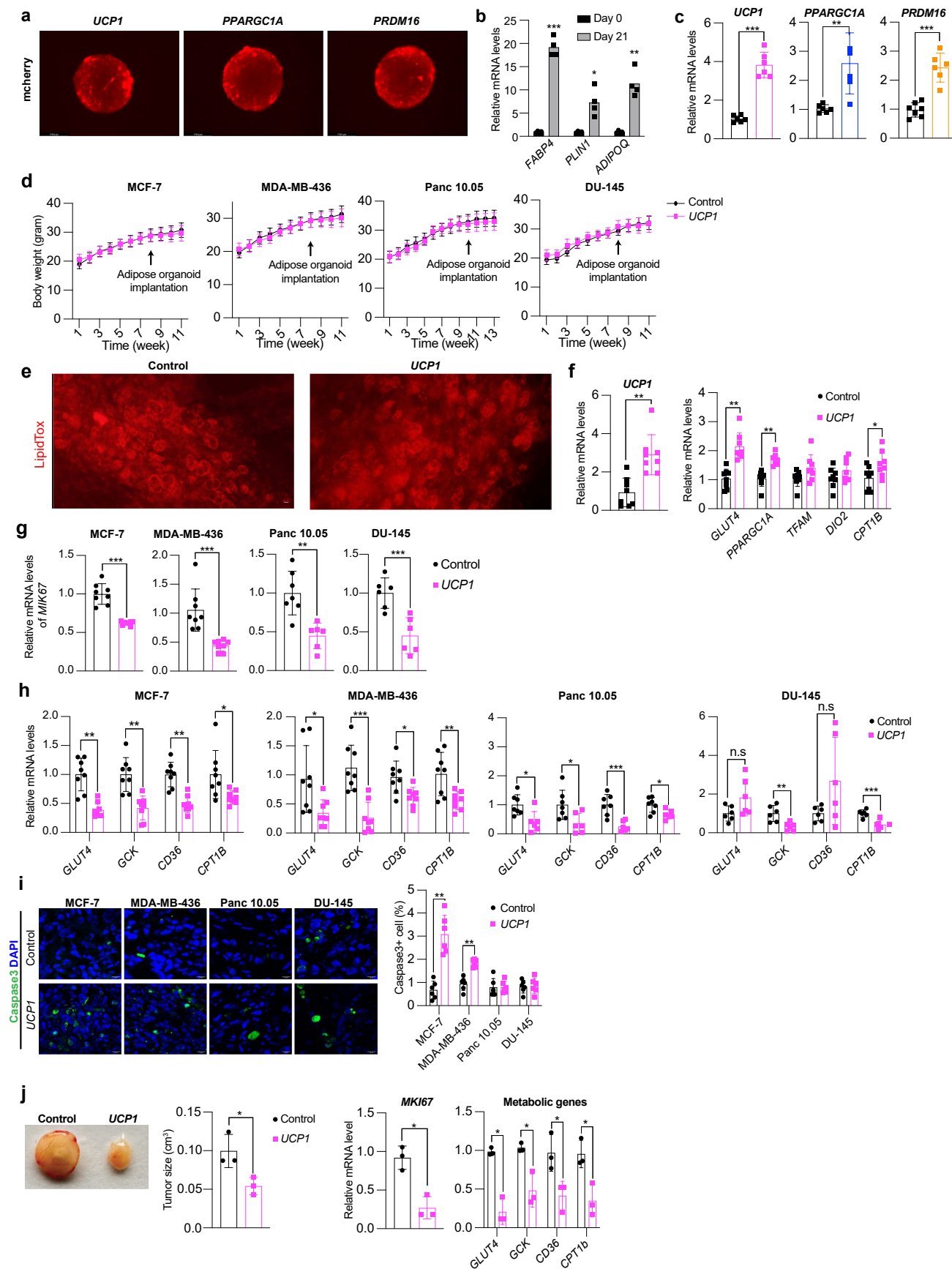
Reprints and permissions information is available at www.nature.com/reprints.



Extended Data Fig. 1 | See next page for caption.

Extended Data Fig. 1 | CRISPRa upregulation of *UCP1*, *PPARGC1A*, and *PRDM16* in human adipocytes suppresses cancer progression in various cancer types.
a, qRT-PCR of *UCP1*, *PPARGC1A*, and *PRDM16* in white adipocytes transfected with CRISPRa using five different gRNAs per gene (n = 2 biological replicates).
b, qRT-PCR of *UCP1*, *PPARGC1A*, and *PRDM16* in human adipocytes transduced by AAV9-CRISPRa with the top two gRNAs per gene (n = 4 biological replicates).
c, qRT-PCR of *UCP1*, *PPARGC1A*, and *PRDM16* in human white adipocytes transduced with CRISPRa targeting *UCP1*, *PPARGC1A*, and *PRDM16* (n = 8–10 biological replicates).
d, qRT-PCR of *TFAM*, *DIO2*, *CPT1b*, and *NRF1* in CRISPRa-modulated adipocytes (n = 8–10 biological replicates).
e, Oxygen consumption rate (OCR) of CRISPRa-modulated adipocytes measured by the seahorse assay (n = 6 biological replicates). Uncoupled OCR was measured under oligomycin treatment, while maximal OCR was measured under FCCP.
f, Glucose uptake of CRISPRa-modulated adipocytes with or without insulin (n = 3 biological replicates).
g, OCR of CRISPRa-modulated cells measured by the seahorse assay in BSA- or BSA-Palmitate- medium (n = 5 biological replicates).
h, Exogenous fatty acid oxidation of CRISPRa-modulated adipocytes calculated by the difference

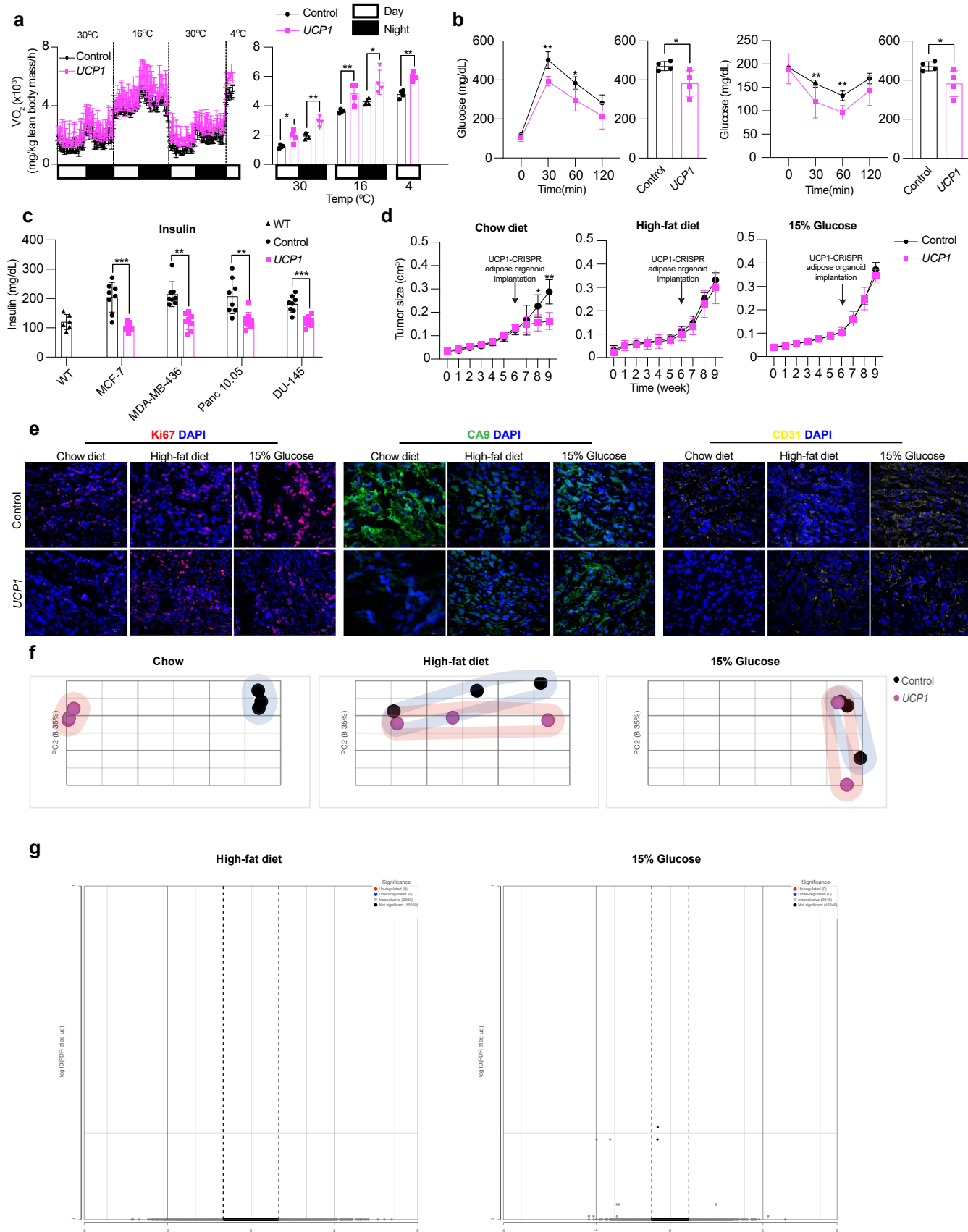
of area under the curve of OCR between BSA- and BSA-Palmitate media upon FCCP treatment (n = 4–5 biological replicates).
i, Fatty acid (FA) uptake of control and *UCP1*-CRISPRa-modulated adipocytes (n = 4 biological replicates).
j, BrdU incorporation of five cancer cell lines co-cultured with CRISPRa-modulated adipocytes (n = 4–5 biological replicates).
k, OCR under FCCP of cancer cells co-cultured with CRISPRa-modulated cells measured by the seahorse assay in BSA- medium (n = 4–5 biological replicates).
l, qRT-PCR (n= 3 biological replicates) and immunoblotting (n = 2 biological replicates; uncropped images in Source Data Extended Data Fig. 1) for *UCP1* in primary adipocytes transduced with *UCP1*-CRISPRa.
m, Cell numbers of various cancer cells co-cultured with CRISPRa-modulated primary adipocytes (n = 5–6 biological replicates).
n, Cell viability assay on MCF-7 cells treated with CRISPRa-*UCP1*-AAV adipocytes (AMT), 6-aminonicotinamide (6-AN; purple bars) at 50 μM, 100 μM and DMSO as negative control and Etomoxir (ETO; yellow bars) at 100 μM, 200 μM and DMSO as negative control (n = 4 biological replicates). All statistical tests in d,e,f,j,k were carried out using a one-way ANOVA and the rest using a two tailed t-test. Data are represented as mean ± standard deviation (SD) *≤0.05, **≤0.01, ***≤0.001.



Extended Data Fig. 2 | See next page for caption.

Extended Data Fig. 2 | CRISPRa upregulation of *UCP1*, *PPARGC1A*, and *PRDM16* in human adipose organoids and proliferation and metabolic gene expression in tumors co-transplanted with CRISPRa-modulated adipose organoids. **a**, Representative images of human adipose organoids transduced with *UCP1*, *PPARGC1A*, and *PRDM16* AAV9 CRISPRa showing mCherry expression. White scale bar on lower left depicts 176.6 μ m. **b**, qRT-PCR of *FABP4*, *PLIN1*, and *ADIPOQ* in adipose organoids (n = 4 biological replicates). **c**, qRT-PCR of *UCP1*, *PPARGC1A*, and *PRDM16* in human adipose organoids transduced by AAV9 CRISPRa (n = 5–7 biological replicates). **d**, Body weight of mice co-transplanted with *UCP1*-modulated adipose organoids and cancer cells (n = 8 mice). **e**, Immunofluorescence of LipidTox-stained adipose organoids after implantation near MCF-7 xenografts. White scale bar on lower right bar depicts 100 μ m. **f**, qRT-PCR of *UCP1*, *GLUT4*, *PPARGC1A*, *TFAM*, *DIO2*, and *CPT1B* of adipose organoids after

implantation near MCF-7 xenografts (n = 8 biological replicates). **g**, qRT-PCR of *MKI67* in xenograft tumors derived from MCF-7, MDA-MB-436, Panc 10.05, and DU-145 cancer cells co-transplanted with *UCP1*-CRISPRa modulated adipose organoids (n = 6–8 biological replicates). **h**, qRT-PCR of *GLUT4*, *GCK*, *CD36*, and *CPT1B* in xenograft tumors (n = 6–8 biological replicates). **i**, Representative images and quantification of immunofluorescence staining for Caspase 3 in tumors co-implanted with *UCP1*-CRISPRa adipose organoids (n = 6 cryosections). White scale bar on lower right bar depicts 10 μ m. **j**, Representative images, volume, qRT-PCR of proliferation marker, *MKI67* and metabolic genes, including *GLUT4*, *GCK*, *CD36*, and *CPT1B* of MCF tumors co-implanted with primary adipose organoids (N = 3 mice). All statistical tests were carried out using a two tailed t-test and data are represented as mean \pm standard deviation (SD) * \leq 0.05, ** \leq 0.01, *** \leq 0.001.

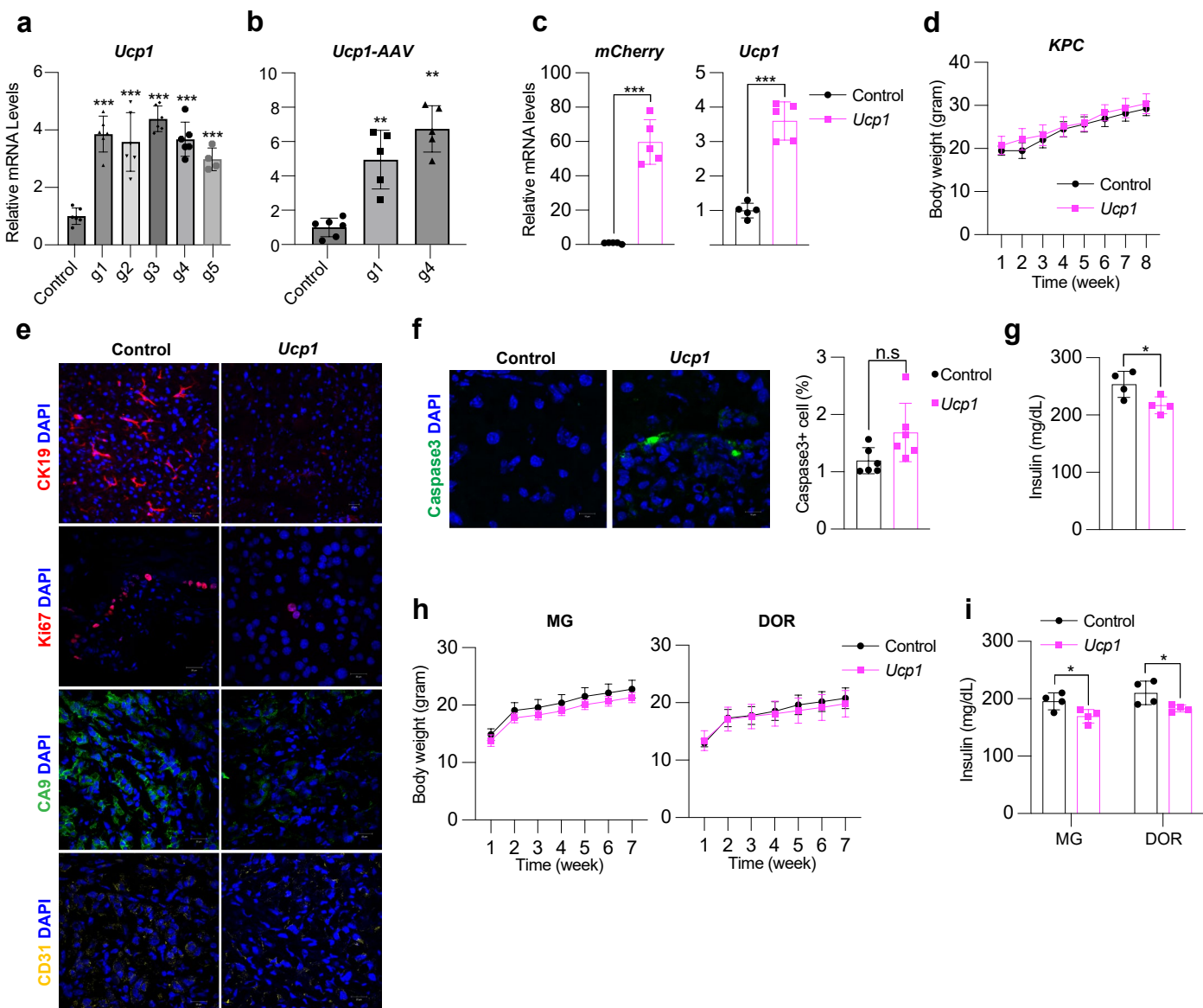


Extended Data Fig. 3 | See next page for caption.

Extended Data Fig. 3 | *UCP1-CRISPRa* human adipose organoids increased whole-body energy expenditure, glucose tolerance, and insulin sensitivity.

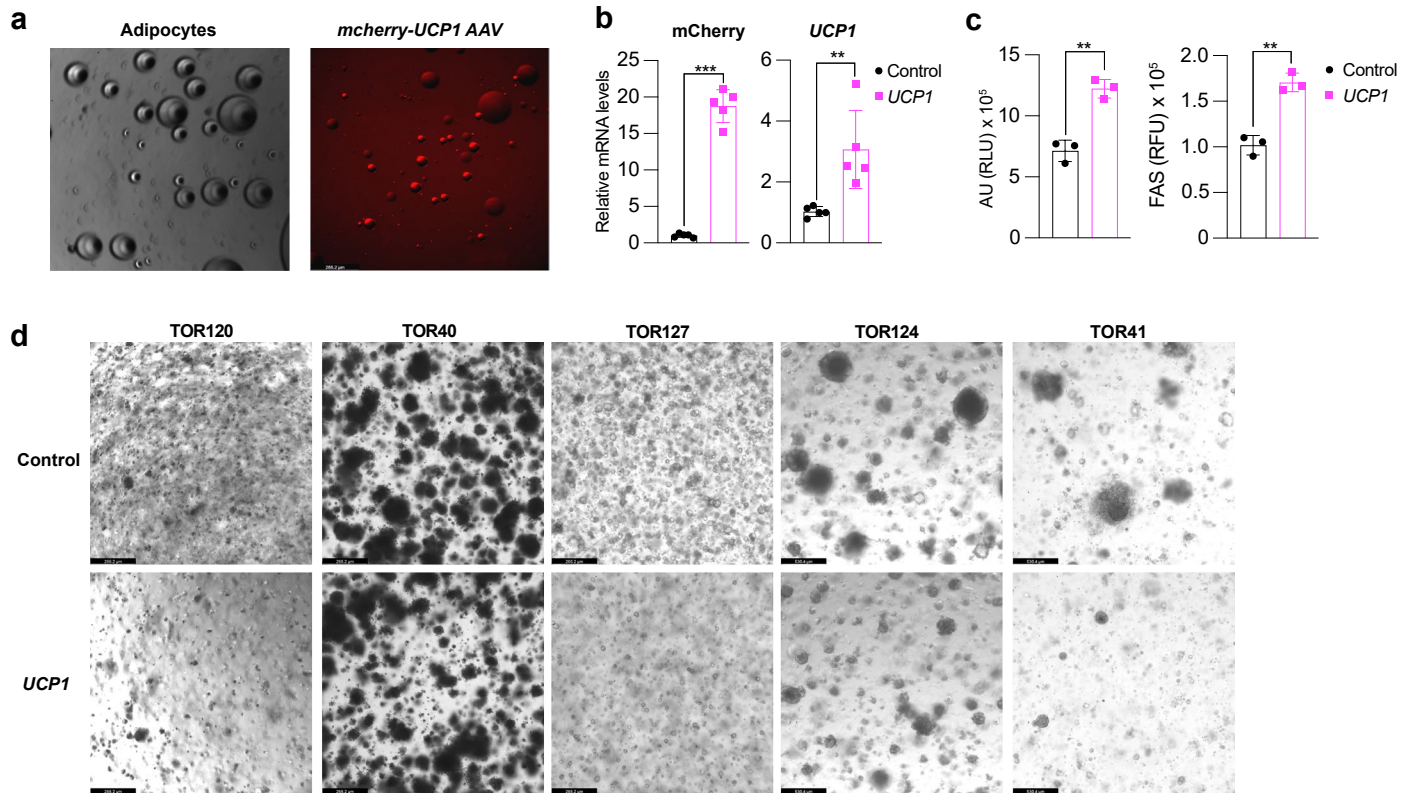
a, Whole-body oxygen consumption at 30 °C, 16 °C, and 4 °C during day and night time of mice implanted with *UCP1-CRISPRa* modulated adipose organoids ($n = 4$ mice). **b**, Glucose tolerance test and insulin tolerance test ($n = 4$ mice). **c**, Plasma insulin levels of wild type SCID mice (WT) and mice that were co-transplanted with dCas9-VP64 (control) and *UCP1-CRISPRa* adipose organoids and xenografts ($n = 6–8$ mice). **d**, tumor size of MCF7 tumor xenograft and *UCP1-CRISPRa* treated human adipose organoids in immune-deficient SCID mice fed with standard chow, high-fat diet (HFD), and 15% glucose containing water during 9 weeks ($n = 4–5$ mice). **e**, Immunofluorescence images from cryosections of xenograft tumors ($n = 5$ sections per treatment) of Ki67, CA9, and CD31. White scale bar on

lower right bar depicts 20 μ m. **f**, Principle component analysis (PCA) of MCF7 tumors that were co-implanted with *UCP1-CRISPRa* treated human adipose organoids in mice fed with standard chow (left) high-fat diet (middle) or 15% glucose (right); ($N = 3$). **g**, Volcano plots showing p-value versus fold change of MCF7 tumors that were co-implanted with *UCP1-CRISPRa* treated human adipose organoids in mice fed with high-fat diet or 15% glucose. No differentially expressed genes were identified, defined as those exhibiting at least a $+/- 4.0$ fold change, with their expression being significantly different from the basal level (false discovery rate (FDR) adjusted, $p < 0.01$). All statistical tests in a-d were carried out using a two tailed t-test and data are represented as mean \pm standard deviation (SD) * ≤ 0.05 , ** ≤ 0.01 , *** ≤ 0.001 .



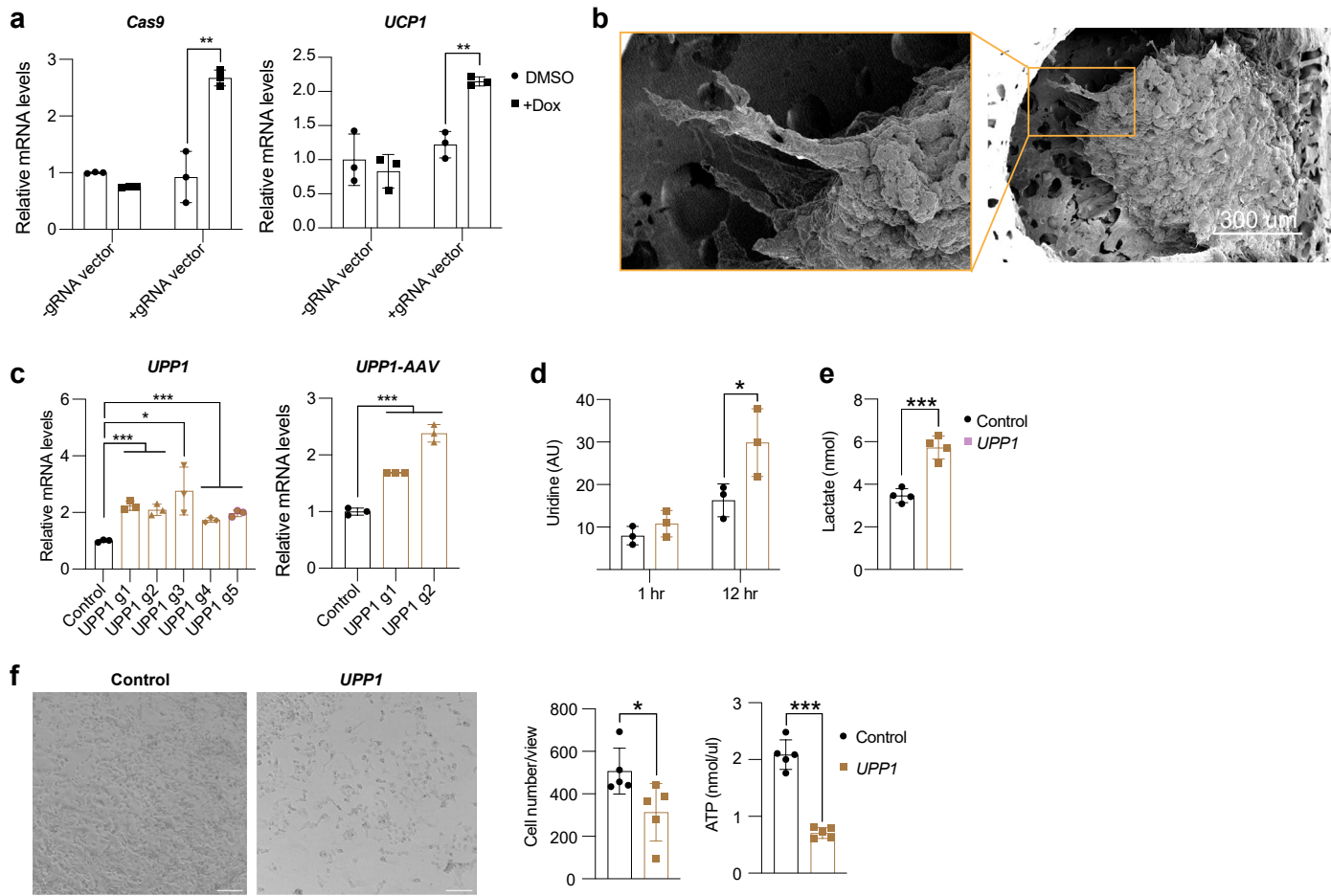
Extended Data Fig. 4 | CRISPRa upregulation of *Ucp1* in mouse white adipocytes and phenotypic analysis of mouse genetic cancer models. **a**, qRT-PCR of *Ucp1* in white adipocytes transfected with CRISPRa using five different gRNAs (n = 4–6 biological replicates). **b**, qRT-PCR of *Ucp1* in mouse adipocytes transduced by AAV9-CRISPRa with two gRNAs (n = 5–6 biological replicates). **c**, qRT-PCR of *mCherry* and *Ucp1* in mouse adipose organoids (n = 5 biological replicates). **d**, Body weight of pancreatic cancer KPC mice implanted with control (dCas9-VP64) or *Ucp1*-upregulated mouse adipose organoids (n = 5–6 mice). **e**, Immunofluorescence staining of CK19, Ki67, CA9, and CD31 in cryosections of pancreatic tumors (N = 6 sections). White scale bar on lower right bar depicts 20µm. **f**, Representative images and quantification of Caspase3+ cells in cryosections.

of pancreatic tumors (N = 6 sections). White scale bar on lower right bar depicts 10µm. **g**, Plasma insulin levels of pancreatic cancer genetic mice implanted with either *Ucp1*-CRISPRa adipose organoids or control organoids (n = 4 mice). **h**, Body weight of breast cancer (MMTV-PyMT) mice implanted with control (dCas9-VP64) or *Ucp1*-CRISPRa mouse adipose organoids nearby mammary gland (MG) or distal (DOR) (n = 4 mice). **i**, Plasma insulin levels of breast cancer genetic mice implanted with either *Ucp1*-CRISPRa adipose organoids or control organoids nearby mammary gland (MG) or distal (DOR) (n = 4 mice). All statistical tests were carried out using a two tailed t-test and data are represented as mean ± standard deviation (SD) * $p \leq 0.05$, ** $p \leq 0.01$, *** $p \leq 0.001$.



Extended Data Fig. 5 | CRISPRa upregulation of *UCP1* in human mammary gland adipocytes. **a**, Representative images of adipocytes isolated from mammary glands that were transduced with *UCP1*-CRISPRa AAV9. Scale bar on lower left depicts 265.2 μ m. **b**, qRT-PCR of *mcherry* and *UCP1* in CRISPRa-modulated mammary gland adipocytes (n = 5 biological replicates). **c**, Glucose uptake and fatty acid uptake of *UCP1*-CRISPRa adipocytes of sample

TOR40 (n = 3 biological replicates). **d**, Bright-field images of adipose organoids that were co-cultured with *UCP1*-CRISPRa modulated mammary gland adipocytes. Scale bars at bottom left depicts 265.2 μ m (TOR40, TOR120, TOR127) and 530.4 μ m (TOR41, TOR124). All statistical tests were carried out using a two tailed t-test and data are represented as mean \pm standard deviation (SD) ** \leq 0.01, *** \leq 0.001.



Extended Data Fig. 6 | Inducible CRISPRa-modulated adipose organoids and CRISPRa-upregulation of *UPP1* in adipocytes to suppress cancer growth of pancreatic ductal adenocarcinoma. **a**, qRT-PCR of *Cas9* and *UCP1* in adipocytes transduced with inducible CRISPRa AAV and treated with either DMSO or doxycycline (Dox) (n = 3 biological replicates). **b**, Electron microscopy image of adipose organoids implanted in a microwell scaffold showing the organoid attached to the scaffold with filopodia and lamellipodia (1.0 kV, 1500x, and 7.861 mm lens). **c**, qRT-PCR of *UPP1* in white adipocytes transfected with CRISPRa using five different gRNAs (left) and AAV transduced (right) with two gRNAs targeting the *UPP1* promoter (n = 3 biological replicates). **d**, Uridine uptake after 1 or 12 hours measured with incubating *UPP1*-CRISPRa modulated adipocytes with 3H-uridine (n = 3 biological replicates). **e**, Lactate levels of *UPP1*-CRISPRa modulated adipocytes (n = 4 biological replicates). **f**, Representative images, cell numbers/view, and ATP levels of PANC-1 cells that were co-cultured with *UPP1*-modulated adipocytes or control (dCas9-VP64 only) adipocytes in high-glucose media (n = 5 biological replicates). White scale bar on lower right bar depicts 100 μm. All statistical tests were carried out using a two tailed t-test and data are represented as mean ± standard deviation (SD) *≤0.05, **≤0.01, ***≤0.001.

targeting the *UPP1* promoter (n = 3 biological replicates). **d**, Uridine uptake after 1 or 12 hours measured with incubating *UPP1*-CRISPRa modulated adipocytes with 3H-uridine (n = 3 biological replicates). **e**, Lactate levels of *UPP1*-CRISPRa modulated adipocytes (n = 4 biological replicates). **f**, Representative images, cell numbers/view, and ATP levels of PANC-1 cells that were co-cultured with *UPP1*-modulated adipocytes or control (dCas9-VP64 only) adipocytes in high-glucose media (n = 5 biological replicates). White scale bar on lower right bar depicts 100 μm. All statistical tests were carried out using a two tailed t-test and data are represented as mean ± standard deviation (SD) *≤0.05, **≤0.01, ***≤0.001.

Reporting Summary

Nature Portfolio wishes to improve the reproducibility of the work that we publish. This form provides structure for consistency and transparency in reporting. For further information on Nature Portfolio policies, see our [Editorial Policies](#) and the [Editorial Policy Checklist](#).

Statistics

For all statistical analyses, confirm that the following items are present in the figure legend, table legend, main text, or Methods section.

n/a Confirmed

- The exact sample size (n) for each experimental group/condition, given as a discrete number and unit of measurement
- A statement on whether measurements were taken from distinct samples or whether the same sample was measured repeatedly
- The statistical test(s) used AND whether they are one- or two-sided
Only common tests should be described solely by name; describe more complex techniques in the Methods section.
- A description of all covariates tested
- A description of any assumptions or corrections, such as tests of normality and adjustment for multiple comparisons
- A full description of the statistical parameters including central tendency (e.g. means) or other basic estimates (e.g. regression coefficient) AND variation (e.g. standard deviation) or associated estimates of uncertainty (e.g. confidence intervals)
- For null hypothesis testing, the test statistic (e.g. F , t , r) with confidence intervals, effect sizes, degrees of freedom and P value noted
Give P values as exact values whenever suitable.
- For Bayesian analysis, information on the choice of priors and Markov chain Monte Carlo settings
- For hierarchical and complex designs, identification of the appropriate level for tests and full reporting of outcomes
- Estimates of effect sizes (e.g. Cohen's d , Pearson's r), indicating how they were calculated

Our web collection on [statistics for biologists](#) contains articles on many of the points above.

Software and code

Policy information about [availability of computer code](#)

Data collection N.A

Data analysis Partek Flow

For manuscripts utilizing custom algorithms or software that are central to the research but not yet described in published literature, software must be made available to editors and reviewers. We strongly encourage code deposition in a community repository (e.g. GitHub). See the Nature Portfolio [guidelines for submitting code & software](#) for further information.

Data

Policy information about [availability of data](#)

All manuscripts must include a [data availability statement](#). This statement should provide the following information, where applicable:

- Accession codes, unique identifiers, or web links for publicly available datasets
- A description of any restrictions on data availability
- For clinical datasets or third party data, please ensure that the statement adheres to our [policy](#)

RNA-seq is available as GEO accession number GSE246231.

Research involving human participants, their data, or biological material

Policy information about studies with [human participants or human data](#). See also policy information about [sex, gender \(identity/presentation\), and sexual orientation](#) and [race, ethnicity and racism](#).

Reporting on sex and gender

N.A

Reporting on race, ethnicity, or other socially relevant groupings

N.A

Population characteristics

N.A

Recruitment

N.A

Ethics oversight

N.A

Note that full information on the approval of the study protocol must also be provided in the manuscript.

Field-specific reporting

Please select the one below that is the best fit for your research. If you are not sure, read the appropriate sections before making your selection.

Life sciences

Behavioural & social sciences

Ecological, evolutionary & environmental sciences

For a reference copy of the document with all sections, see nature.com/documents/nr-reporting-summary-flat.pdf

Life sciences study design

All studies must disclose on these points even when the disclosure is negative.

Sample size

Sample size of at least 2 for cells or 4 for mice was selected based on variance observed in prior experiments of a similar nature, as well as practical considerations.

Data exclusions

Data were not exclude from analysis.

Replication

To ensure robust reproducibility, all data presented in the manuscript were repeated at least three times (two times only for initial CRISPRa sgRNA transfection guide selection). All replication attempts were successful.

Randomization

N.A

Blinding

No blinding was performed in this study. It required to use the correct genotypes of cells and mice

Reporting for specific materials, systems and methods

We require information from authors about some types of materials, experimental systems and methods used in many studies. Here, indicate whether each material, system or method listed is relevant to your study. If you are not sure if a list item applies to your research, read the appropriate section before selecting a response.

Materials & experimental systems

n/a	Involved in the study
<input type="checkbox"/>	<input checked="" type="checkbox"/> Antibodies
<input type="checkbox"/>	<input checked="" type="checkbox"/> Eukaryotic cell lines
<input checked="" type="checkbox"/>	<input type="checkbox"/> Palaeontology and archaeology
<input type="checkbox"/>	<input checked="" type="checkbox"/> Animals and other organisms
<input checked="" type="checkbox"/>	<input type="checkbox"/> Clinical data
<input checked="" type="checkbox"/>	<input type="checkbox"/> Dual use research of concern
<input type="checkbox"/>	<input checked="" type="checkbox"/> Plants

Methods

n/a	Involved in the study
<input checked="" type="checkbox"/>	<input type="checkbox"/> ChIP-seq
<input checked="" type="checkbox"/>	<input type="checkbox"/> Flow cytometry
<input checked="" type="checkbox"/>	<input type="checkbox"/> MRI-based neuroimaging

Antibodies

Antibodies used

Ki67 (SolA15),Fisher Scientific,14-5698-82
Carbonic Anhydrase,Fisher Scientific,AF2188
CD31,Fisher Scientific,BBA7

GAPDH, Cell Signaling, 5174
 Goat anti-rat, Alexa Flour 647, Fisher Scientific, A21247
 Goat anti-mouse, Alexa Fluor 594, Life Technologies, A11032
 Donkey anti-goat, Alexa Fluor 594, Fisher Scientific, A11055
 Caspase 3, Cell Signaling, CS9661
 CK19, Abcam, Ab203444
 UCP1, R&D, MAB6158

Validation

Ki67- [https://www.thermofisher.com/antibody/product/Ki-67-Antibody-clone-SolA15-Monoclonal/14-5698-37?glcid=Cj0KCQjw27mhBhC9ARlsAlFsETEvjm59r_6344DC3_jxeeelBcjHtvUN6FV_e1JxDJyqy8Z0Ns9dsalaAhu-EALw_wcB&ef_id=Cj0KCQjw27mhBhC9ARlsAlFsETEvjm59r_6344DC3_jxeeelBcjHtvUN6FV_e1JxDJyqy8Z0Ns9dsalaAhu-EALw_wcB:G:s&s_kwcid=AL!3652!3!278870232429!!g!!!1454324556!](https://www.thermofisher.com/antibody/product/Ki-67-Antibody-clone-SolA15-Monoclonal/14-5698-37?glcid=Cj0KCQjw27mhBhC9ARlsAlFsETEvjm59r_6344DC3_jxeeelBcjHtvUN6FV_e1JxDJyqy8Z0Ns9dsalaAhu-EALw_wcB&ef_id=Cj0KCQjw27mhBhC9ARlsAlFsETEvjm59r_6344DC3_jxeeelBcjHtvUN6FV_e1JxDJyqy8Z0Ns9dsalaAhu-EALw_wcB:G:s&s_kwcid=AL!3652!3!278870232429!!g!!!1454324556!63404918784&cid=bid_pca_frg_r01_co_cp1359_pjt0000_bid00000_ose_gaw_dy_pur_con)
 CA9-https://www.rndsystems.com/products/human-carbonic-anhydrase-ix-ca9-antibody_af2188
 CD31-https://www.rndsystems.com/products/human-cd31-pecam-1-antibody-9g11_bba7?glcid=Cj0KCQjw27mhBhC9ARlsAlFsETESGafo_oT07Q0oQcgGzrDCU8jmY4a2yrbTsHU1rGsCo_SF41YaAsWdEALw_wcB&gclsrc=aw.ds
 Caspase3-<https://www.cellsignal.com/products/primary-antibodies/cleaved-caspase-3-asp175-antibody/9661>
 CK19- <https://www.abcam.com/products/primary-antibodies/alexa-fluor-555-cytokeratin-19-antibody-ep1580y-ab203444.html>
 GAPDH- <https://www.cellsignal.com/products/primary-antibodies/gapdh-d16h11-xp-rabbit-mab/5174>
 UCP1- https://www.rndsystems.com/products/human-mouse-ucp1-antibody-536435_mab6158

Eukaryotic cell lines

Policy information about [cell lines and Sex and Gender in Research](#)

Cell line source(s)

Human preadipocyte cell line was obtained from Dr. Hei Sook Sul lab at UC Berkeley. It was generated by immortalizing human male subcutaneous preadipocytes. DU-415, Panc 10.01, SW-1417, MDA-MB-436, MCF7 and Mouse 3T3-L1 were obtained from ATCC. AAVpro 293T cells were obtained from Takara.

Authentication

Preadipocyte cell lines were subjected adipocyte differentiation and adipogenic markers were checked with qRT-PCR.

Mycoplasma contamination

All lines were tested for mycoplasma.

Commonly misidentified lines
(See [ICLAC](#) register)

N.A

Animals and other research organisms

Policy information about [studies involving animals; ARRIVE guidelines](#) recommended for reporting animal research, and [Sex and Gender in Research](#)

Laboratory animals

SCID mice (JAX, 001303), FVB/N-Tg(MMTV-PyVT)634Mul/J (JAX, 002374), Krastm4Tyj Trp53tm1Brn Tg(Pdx1-cre/Esr1*)#Dam/J (Jax, 032429)

Wild animals

N.A

Reporting on sex

We used both males and females

Field-collected samples

N.A

Ethics oversight

UCSF Institutional Animal Care & Use Program

Note that full information on the approval of the study protocol must also be provided in the manuscript.